Materials Today Advances 8 (2020) 100108

Contents lists available at ScienceDirect

Materials Today Advances

journal homepage: www.journals.elsevier.com/materials-today-advances/

Progress and prospects of two-dimensional materials for membrane-based water desalination

J. Safaei [a], P. Xiong [b, **], G. Wang [a, *]

[a] Centre for Clean Energy Technology, School of Mathematical and Physical Sciences, University of Technology Sydney, Sydney, NSW 2007, Australia
[b] Key Laboratory of Soft Chemistry and Functional Materials, Ministry of Education, Nanjing University of Science and Technology, Nanjing 210094, China

ARTICLE INFO

Article history:
Received 7 July 2020
Received in revised form
7 August 2020
Accepted 12 August 2020
Available online 19 September 2020

Keywords:
2D materials
Nanosheets
Water purification
Interlayer distance
Ion sieving

ABSTRACT

Water scarcity is one of the most critical issues of this century. Currently, water desalination is performed using polymeric membranes. However, the polymers suffer from low water permeability and degradation, both of which increase energy consumption and the cost of water desalination. There have been several breakthroughs by deploying two-dimensional (2D) materials with the merits of excellent water permeability and chemical resistance, rendering them highly promising as alternative materials of choice for water desalination. However, controlling and maintaining the pores and channels of 2D-based membranes down to the subnanometer level is a challenging process. Herein, we summarized the research progress on 2D materials for membrane-based water desalination. Several nanoporous and stacked membranes of 2D materials are discussed. Design strategies to maintain the stability of the membranes are particularly elucidated, including pore size optimization and interlayer spacing engineering down to subnanometer scales. The current challenges and future research directions are also presented.

1. Introduction

One of the unrelenting global issues in the21st century is the inadequate availability of clean water. Rapid urbanization, population growth, and climate change directly account for freshwater scarcity on our planet [1,2]. Half of the world's population live in the close vicinity of oceans that cover 80% of the earth's water supply. Hence, seawater desalination could solve the world's water shortages problems, especially in the areas where ground or spring water is not available [3–5]. Water desalination based on membranes is one of the most energy-efficient approaches currently implemented in the industry [6].

Membranes generally act like sieves where water molecules are permeated while dissolved salt ions are blocked. The first step in designing membranes is to identify the substances to be removed. Sodium (Na^+) and chloride (Cl^-) ions (i.e. monovalent ions) form 85% of seawater minerals, with magnesium (Mg^{2+}), calcium (Ca^{2+}) and sulfate (SO_4^{2-}) ions (i.e. divalent ions), together counting 12% [7]. Hence, the separation of monovalent ions removes the majority of the ions from seawater and makes it drinkable. However, monovalent ions are significantly more challenging to filter out than divalent ions due to their smaller size [8]. The separation of monovalent ions via membrane-based technique requires materials that have pores/channels with sizes of less than 1 nm (i.e. subnanometer scales) [9].

Currently, the principle filtration technique in the commercial market is based on thin-film composite membranes, where the dense polyamide layer with its subnanometer pores is responsible for blocking monovalent ions [10]. However, polyamide has several drawbacks, such as low water permeability and degradation [11]. Generally, the polymeric membranes suffer from weak chemical resistance, limited lifetime, and membrane fouling [12]. These issues have forced researchers to pursue inorganic materials that have the merits of outstanding water permeability, thermal stability, solvent resistance, and durability [13–15]. Several inorganic materials such as zeolites [16,17], and carbon nanotubes [18], have been employed for water desalination due to their subnanometer pores/channels. However, the high cost- and time-consuming process in preparing perfectly ordered subnanometer arrays of zeolites and carbon nanotubes hinder their commercialization for water desalination [19].

* Corresponding author.
** Corresponding author.
E-mail addresses: pan.xiong@njust.edu.cn (P. Xiong), guoxiu.wang@uts.edu.au (G. Wang).

https://doi.org/10.1016/j.mtadv.2020.100108

As another alternative to polymeric membranes, 2D materials are actively sought after since they can achieve ions-sieving either via in-plane pores or channels of stacked nanosheets, both of which can be economically produced at large-scales. The hyper-thinness of 2D monolayers renders possible the fabrication of ultrathin membranes with excellent mass transport and high water flux [19–23]. Besides, 2D materials can significantly enhance the solute-solute selectivity due to their structural and chemical homogeneity [9]. 2D materials are well-known for nanofiltration membrane applications (i.e. molecular and divalent ions sieving with sizes above 1 nm) [24,25]. Several review articles have summarized 2D materials for molecular sieving and nanofiltration applications [26–29]. However, most of them lack the implementation of 2D materials, specifically for monovalent ion sieving. This is because controlling and maintaining the pore/channel sizes of 2D-based membranes down to the subnanometer level is a challenging process. There have been several profound scientific breakthroughs in tuning the pores and interlayer distances of 2D materials down to the subnanometer scale [30–32]. Furthermore, new 2D materials and novel techniques have enabled electrostatic exclusion capabilities, leading to monovalent ion sieving without the need for subnanometer scale size-tuning [33,34]. Thus, it is essential to review the 2D materials and nanotechniques for obtaining monovalent ion sieving via pores, nanochannels, and electrostatic repulsion effects for desalination.

In this review, we overviewed the recent progress on 2D material-based membranes for water desalination. We first discussed the mechanism of water desalination across 2D materials. Then, two types of nanoporous and stacked membranes were summarized together with the underlying challenges of optimizing pores and channels down to the subnanometer scale. Finally, we proposed future research directions for the implementation of 2D materials for water desalination. It is envisioned that membrane-based water desalination could be significantly energy-efficient and low-cost upon employing 2D materials.

2. Mechanism of water desalination in 2D materials

It is crucial to understand the diffusion of water molecules or solutes and solvents for designing desalination membranes. For any membrane, regardless of its type, the transportation of water is governed by the solution-diffusion model, Eq. (1):

$$J_W = A(\Delta P - \Delta \pi_m) \quad (1)$$

where J_W is the volumetric water flux, A is water permeability coefficient (permeance), ΔP is the applied hydraulic pressure, and $\Delta \pi_m$ is the osmotic pressure difference between feed and permeate side. In reverse osmosis (RO), the water flow is driven by hydraulic pressure, whereas in forward osmosis (FO), the osmotic pressure drives the stream via a highly concentrated draw solution. Hence, increasing either external pressure on the feed solution in RO mode, or raising the concentration of draw solution in FO mode accelerates the diffusion of solute molecules across the membrane.

The solute flux can be modelled using Fick's law of diffusion, Eq. (2):

$$J_s = B\Delta c_m \quad (2)$$

where J_s is the solute flux, B is solute permeability coefficient, and Δc_m is the solute concentration difference across the membrane. From Fick's law, it is concluded that regardless of FO or RO operation, increasing the concentration of feed solution accelerates solvent diffusion across membranes. Eqs (1) and (2) clearly show the contribution of the membrane's active layer towards solvent/solute permeability via A and B coefficients. For commercial membranes, these coefficients can be tailored via changing the thickness of the polyamide layer. Usually, commercial polyamide layers have a thickness of ~150 nm. Reducing the width of the selective layer results in higher water permeability, but it comes at the expense of higher salt permeability (i.e. low salt rejection). Hence, the control of compactness, thickness, and chemistry of polyamide layers considerably affects desalination performance [11].

For 2D materials, the mechanisms are identical, except instead of dense polyamide layers, the nanosheets perform the selective mass transportation. Ion sieving can be achieved either via drilling subnanometer pores on the surfaces of nanosheets, or nanochannels from the stacked membranes (Fig. 1a, d). Selective mass transport through the 2D materials-based membranes for desalination is mainly achieved via two principal mechanisms, e.g. size exclusion and Donnan electrostatic exclusion. Based on the size-exclusion mechanism, the water molecules of smaller sizes are permeated while hydrated ions are blocked. In 2D materials, water desalination via size exclusion can be achieved either through the in-plane nanopores on single monolayers (Fig. 1b) or as stacked nanosheets on top of one another with the nanochannels in between (Fig. 1e) [21]. The second principle mechanism is due to the electrostatic Donnan exclusion effect, where electrically charged surfaces block the hydrated ions [35]. Regardless of stacked or nanoporous membranes, the Donnan effect plays a crucial role in selective transportation. In this case, surface electrostatic charges block ions either on the pore edges of the nanopores (Fig. 1c) or on the line edges and surfaces of nanosheets (Fig. 1f).

For stacked membranes, increasing the interlayer distances also increases J_W followed by the increase in salt diffusion J_s. Whereas for nanoporous membranes, J_W and J_s is directly proportional to the pore sizes. Hence, to achieve selective mass transfer and to obtain the optimum selectivity (J_s) /permeability (J_W) trade-off, one should optimize the pore size of the nanoporous membranes or tune the interlayer distances of the stacked nanosheets. The surface chemistry and polarity of the nanopores and nanosheets could also alter salt rejection performance. Although we mainly focus on the techniques for tuning interlayer distances of stacked membranes in this article, we also briefly discuss the effect of surface chemistry and Donnan exclusion in the last section of this review.

3. Nanoporous membranes

Nanoporous membranes are highly promising due to their atomic thickness, which decreases solute diffusion friction dramatically, resulting in impressive water permeability. Tuning pore sizes below the sizes of the hydrated ions would render possible the application of these membranes for monovalent ion removal [14,36,37]. In this section, 2D materials with externally drilled pores (extrinsic pores) and ingenious/intrinsic pores for water desalination applications are discussed.

3.1. Extrinsic pores

Developing nanopores on monolayers of 2D materials is a unique technique to produce membranes with ultra-high water permeability. Parameters such as defects [30,38,39], pore size [30,39], pore surface chemistry [40,41], and mechanical strength of nanoporous monolayers [42,43] are essential to consider for practical applications.

O'Hern et al. grew defective graphene via CVD and bombarded it with gallium ions. Before gallium ion bombardment, the defects were sealed using polymers and atomic layer deposition (ALD)-coated hafnium oxide. This membrane, however, showed relatively low water permeability and salt rejection rates, especially for NaCl.

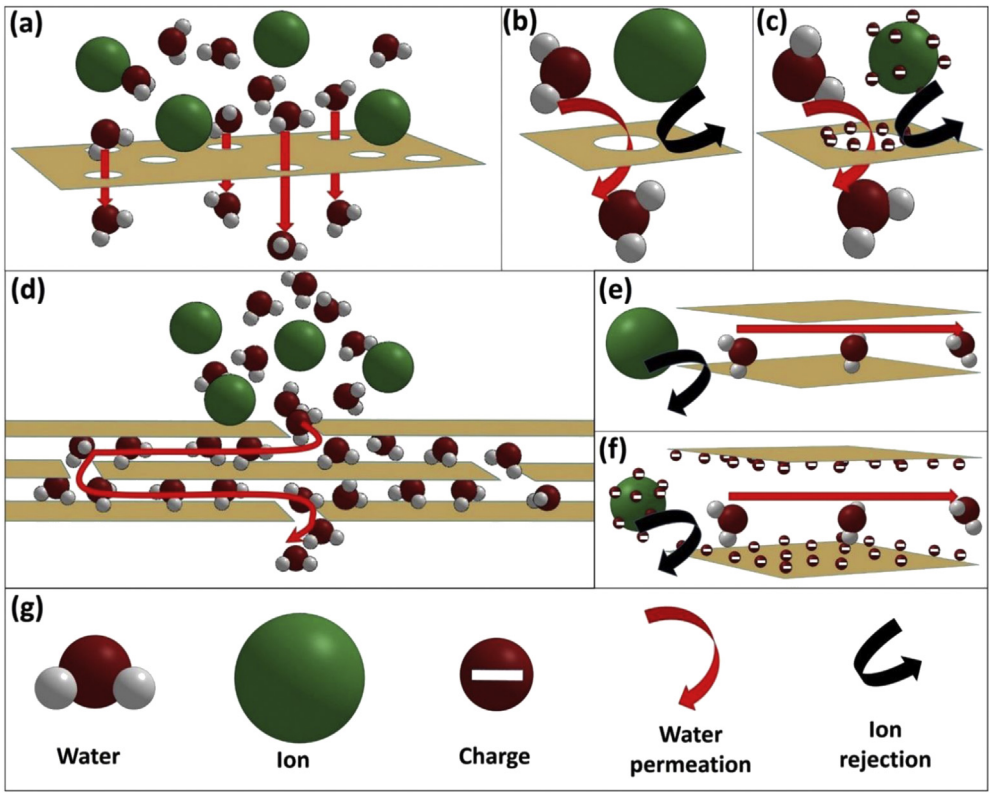

Fig. 1. Mechanism of water desalination in 2D materials. Water molecules across a) in-plane nanopores of monolayers, and d) nanochannels of stacked nanosheets. The ions are blocked via size exclusion effect on 2D materials via their b) nanopores, and e) interlayer spacing. The Donnan electrostatic exclusion effect of ions via c) nanoporous 2D materials, and f) 2D nanochannels of stacked nanosheets. g) The symbols of the water molecule, ion, electrostatic charge, water permeation, and ion rejection.

The low salt rejection and low water permeability could be correspondingly pertinent to undesired defects, which could not be perfectly sealed and the nature of the nanopore chemistry, respectively [39]. Growing defect-free graphene, however, resulted in membranes with much better performances that should be taken into account upon realizing these types of membranes [30,43].

To produce pores on graphene, O'Hern et al. utilized the Gallium ions bombardment technique. This technique yielded sub-nanometer pores with a mean diameter of 0.152 nm with no holes larger than 0.5 nm. These pore sizes could theoretically permeate water molecules while blocking salt ions (van der Waals diameter of the water molecule and hydrated salt ions are approximately 0.275 nm and 0.7 nm, respectively). The membrane demonstrated 1.51 L/m^2/h/bar (LMHB) flux with a 70% rejection of $MgSO_4$. There is no report on tuning pore sizes via the traditional Gallium ions bombardment technique [39]. Deploying oxygen plasma technique, however, could solve this issue, leading to pores of various sizes [30,43]. In one study, Surwade et al. grew defect-free graphene and deployed oxygen plasma as a method to generate subnanometer pores. This strategy yielded ultra-high water flux as high as 70 g/m2/s/atm (254 LMH) that is significantly higher than theprevious research by a considerable degree and also among the highest ever reported (Table 1). The pore formation could be studied using Raman plot via the ratio I_D to I_G, which is a widely recognized technique to measure defects in graphene [44]. Increasing plasma etching time increased the I_D/I_G ratio, and also reduced the length of neighboring pores. However, excess of plasma exposure eliminated the 2D nature of carbon, producing amorphous carbon due to the elimination of the 2D peak (Fig. 2a) [30].

The nature of pore chemistry either depends on the external factor such as pore fabrication technique [30,39,43], or ingenuine properties of the materials [19,41]. Although having the same sizes, the pores developed by oxygen plasma demonstrated higher water permeability compared to those produced by Gallium Ions bombardment [30,43]. It is stated that the surface chemistry of the pores dominates the water structure in the nanopores [45]. In a theoretical simulation by Cohen et al. the hydroxyl functional groups on the edges of nanopores could roughly double the water flux due to their hydrophilic character [40]. Hence, it is arguable that oxygen plasma could have hydroxylated the pores, dramatically enhancing the water flux. Deployment of other nanopore fabrication techniques such as chemical etching [46], electrochemical reactions [47], annealing under oxygen [48], and chemical oxidations [49] could also alter pore chemistry, demanding further investigations.

As another factor that alters the nature of pore chemistry is the intrinsic elemental features of 2D materials [19,41]. As an alternative to graphene monolayers, transition metal dichalcogenides (TMDs) could also be promising for this application due to their both surfaces being exposed to sulfur atoms, rendering them highly hydrophilic with high affinity for water molecules [19]. Heiranian et al. theoretically simulated water desalination through nanoporous molybdenum disulfide (MoS_2). The results proved that the membranes could obtain 70% higher water flux compared with graphene nanopores while maintaining 88% ions rejection rate. More specifically, of the three pore configurations of molybdenum only, sulfur only, and mixed, the molybdenum-only pores showed the highest water velocity and also water density. This performance was ascribed to be due to the hydrophilic nature of molybdenum as it attracts water to the pore interior (Fig. 2b–d) [41].

One of the most important problems to tackle with these membranes is the mechanical fragility due to the atomic-layer thickness of the nanosheets. In one insightful study by Ferrari

Table 1
Performance comparison of 2D material membranes for water desalination.

Membrane Classification			Membrane Materials	Preparation Technique	Salt rejection rate[a]	Water flux[a]	Stability	Test condition[a,b]	Ref.
Nanoporous			Single-layer nanoporous graphene@ single-walled carbon nanotubes	CVD followed by oxygen plasma etching for subnanometer pore generation	87%	97.6 LMHB	24 h	2,000 ppm NaCl (cross-flow reverse osmosis)	[43]
			Subnanometer porous monolayered graphene	CVD followed by Gallium ion bombardment	~10% for [16.6 mM NaCl/glycerol ethoxylate]	~33 LMH	N/A	[glycerol ethoxylate/de-ionized (DI) water] FO (~25 atm)	[39]
			Single-layer nanoporous graphene	CVD followed by oxygen plasma etching for subnanometer pore generation	100%	254 LMHB	25 h	[DI water/1 M KCl] (FO)	[30]
			Metal-organic framework	Exfoliation of the bulk layered structure	~100%	0.04 LMHB	750 h	[DI water/0.5 M NaCl] (FO)	[57]
Stacked	Unmodified		Few-layered MoS_2	Chemical vapor deposition	99.5% [DI water/0.1 M NaCl] (FO)	322 LMHB	1.78% salt rejection degradation after 24 h	DI water (dead-end) under 1 bar	[98]
			MXene	Vacuum filtration (self-cross-linked by heating)	99%	0.06 LHMB	70 h	[DI water/0.2 M NaCl] (FO)	[34]
			rGO and reduced by HI (Free-standing)	Vacuum filtration	0.2 mol^{-1} h^{-1} m^{-2} [0.1 M NaCl/0.5 M NH_4HCO_3] (FO)	57.0 LMH	N/A	[DI water/2 M NaCl] (FO)	[69]
			rGO laminates (Interlayer spacing control using humidity control)	Physical binding using epoxy (free-standing)	97%	0.5 LMH	20 h	0.1 M NaCl/3 M sucrose (FO)	[32]
			MoS_2 modified by organic dyes	Vacuum filtration	99% [0.1 mM/1 M NaCl] (FO)	262 LMHB	8% salt rejection degradation after 3 h	1 M NaCl under 1 bar (dead-end)	[97]
			PDDA-functionalized GO	Pressure Filtration (~3 bar)	96%	14 LMH	120 h	50 ppm Na_2SO_4 (dead-end)	[35]
			Methyl-functionalized MoS_2	Vacuum filtration	87%	80 LMH (dead-end) under 4 bar	15 h (20% water flux reduction)	[0.1 M NaCl/3 M KCl] (FO)	[100]
	Modified	Metal ions	GO cross-linked by K^+ ion	Drop casting (free-standing)	2.7 × 10^{-2} mol/h/m^2	0.1 LMH	5 h	[0.25 M KCl/0.25 M KCl + 0.25 M NaCl] (FO)	[75]
			K^+ ion-modified GO	Doctor blade casting (free-standing)	82%	100 LMH	80 min (37% water flux reduction)	100 mgL NaCl (dead-end) under 1 bar	[76]
			Al^{3+}-ions intercalated Ti_3C_2Tx MXene	Vacuum filtration	96.5%	2.8 LMH	400 h	[2 M sucrose/0.1 M NaCl	[77]
		Monomers	GO cross-linked by EDA	Vacuum filtration	36.3%	4.1 LMH	N/A	1,000 ppm NaCl (dead-end) under 1 bar	[81]
			MPD-TMC cross-linked GO	Pressure Filtration (5 bar)	~1.5 g/h/m^2	~18 LMH	350 min (1.3% water flux reduction)	[DI water/2 M NaCl] (FO)	[82]
		Polymers	GO cross-linked with polymer	Spin coating (Free radical polymerization)	99.9%	25.8 LHM	Few weeks	[DI water/1 M NaCl] (FO)	[85]
			GO cross-linked with polymer	Vacuum filtration (Free radical polymerization)	98.5%	35.6 LHM	N/A	[2,000 ppm NaCl/DI water] (RO under 10 bar)	[86]

[a] ('Salt rejection rate' and 'Water flux' are tested under identical conditions (i.e. 'Test condition' column) unless stated otherwise. In that case, 'Test condition' is pertinent to 'Water flux'.).
[b] (The forward osmosis (FO) is represented as [A/B], where A is the feed solution, and B is the draw solution.).

et al. in-situ atomic force microscopy (AFM) technique demonstrated that monolayers of graphene could completely swell and soften upon introducing and removing water in a microfluidic system. The swelling of graphene could be up to (~tens of nanometers), and graphene could also retain its intrinsic elastic properties upon contact with water [42]. This study demonstrates the excellent mechanical properties of the monolayer graphene for various membrane applications. Although monolayer graphene is strong, the formation of defects and nanosized pores could deteriorate its mechanical properties for membrane applications [21]. This issue, however, can be solved by deploying an interconnected matrix of nanotubes [43]. Considering all the mentioned strategies, Yang et al. grew defect-free graphene, developed nanopore via oxygen plasma etching, followed by incorporation with single-walled carbon nanotube (SWCNT) backbone, simultaneously solving the issues faced by defects, pore sizes, pore chemistry and also mechanical stability. Inspired by the structures of plant leaves, nanoporous graphene monolayer was incorporated into SWCNT as

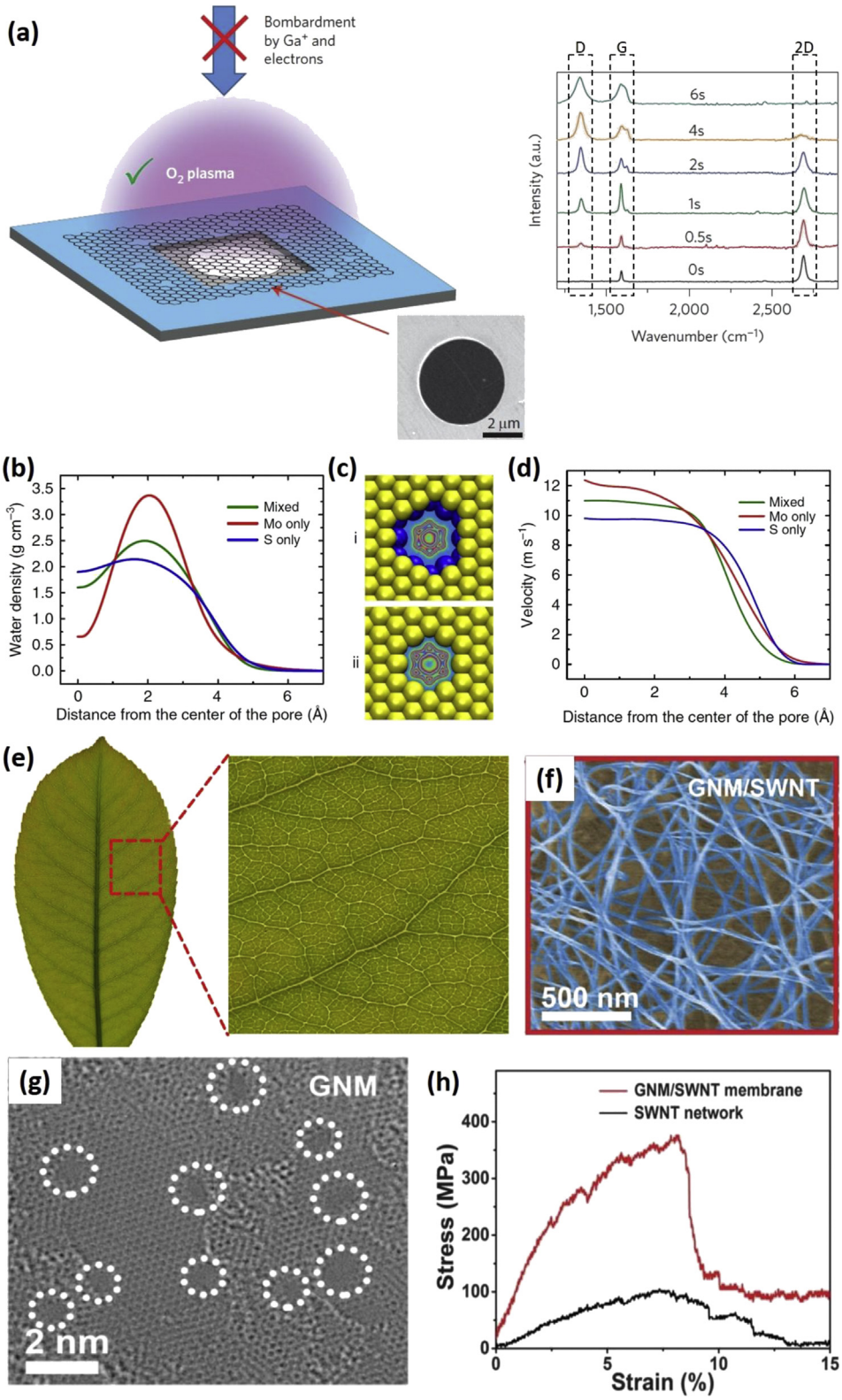

Fig. 2. a) Oxygen plasma etching of graphene monolayer as an effective nanopore fabrication technique, together with the Raman spectra under different plasma etching time. Reproduced with permission [30]. Copyright 2015, Nature Publishing Group. The effect of pore chemistry for nanoporous MoS_2 membrane, depicting b) water distribution in the radial direction with different pore chemistry, c) density map of water distribution for (i) Mo only and (ii) S only pores, and d) the velocity of water molecules as a function of distance from the center of the nanopore. Reproduced with permission [41]. Copyright 2015, Nature Publishing Group. Nature-mimicking fabrication of graphene incorporated with SWCNT, showing e) the structure of the plant leaves, f) scanning electron microscopy (SEM) image, g) aberration-corrected scanning transmission electron microscopy (STEM) image, and h) stress-strain of SWCNT and its composite with graphene under uniaxial tensile strength. Reproduced with permission [43]. Copyright 2019, American Association for the Advancement of Science (AAAS).

mechanical support. They first integrated monolayer defect-free graphene into SWCNT, followed by oxygen plasma etching under various times. Tunablepore sizes of ~0.55, ~0.63, and ~1.41 nm were achieved proportional to plasma etching time. Furthermore, 80% of the pores had sizes ranging from ~0.5 to 0.75 nm, representative of their uniform distribution [43]. In fact, pore homogeneity is a crucial parameter since uniform pore distribution would reduce pressure difference due to lessened frictional loss and pressure drop across the membrane [50]. Interestingly, the tensile strength of the SWCNT was also enhanced via incorporation with the monolayer graphene (Fig. 2e–h). Water and salt permeance increased proportionally to the plasma etching time. The 10 s of plasma etching resulted in water permeance of 20.6 LMHB and NaCl rejection of 98.1%, which was stable for 24 h of the test. The membranes were also tested under reverse osmosis cross-flow filtration system, demonstrating an outstanding water flux of 97.6 LMHB and a reasonable salt rejection rate of more than 85% [43].

From the studies mentioned above, we can infer that the fabrication of uniform and defect-free graphene is the first step to block the movement of unwanted ions. What's more, the technique of nanopore formation could alter the nature of pore chemistry, which has a consequential effect on water permeability. And lastly, the mechanical fragility of the monolayers can be solved via the incorporation of carbon nanotubes backbone. Although theoretical studies demonstrate excellent potentials of TMD's, no experimental research has been performed on these types of membranes until now. Recently Thiruraman et al. and Ryu et al. demonstrated the fabrication of atomic vacancies fabricated in molybdenum disulfide (MoS_2) and tungsten disulfide (WS_2) [51,52]. These experiments could lay the foundation for deploying TMD monolayers with subnanometer pores for water desalination applications.

3.2. Intrinsic pores

Although most of the research are devoted to developing extrinsic pores on monolayers, less focus is put forward on materials with intrinsic pores. Materials with built-in pores not only eliminate the tedious pore fabrication process but also results in higher mechanical strength and filtration performance. In this regard, scientists studied various materials such as the family of covalent triazine frameworks [53,54], metal-organic frameworks (MOF) [55–57], and graphynes [58–61] for water desalination.

Some materials, such as the family of covalent triazine frameworks (CTF), more widely known as graphitic carbon nitride (g-C_3N_4), have the intrinsic in-plane nanopores that theoretically enable the sieving of monovalent ions [53,54]. Favored by the high chemical and structural stability of g-C_3N_4, Lin et al. theoretically simulated water desalination across CTF with various configurations (Fig. 3a). In order to reduce the effective pore size, two types of chemical functional groups of $-Cl$ and $-CH_3$ were further added. Due to the negative charges of $-Cl$ functionalized CTF (CTF-Cl) that attracts the positive sodium ions, this membrane showed lower salt rejection of 96% compared with the non-polar $-CH_3$ functionalized CTF (CTF-CH_3) with 100% salt rejection. The water permeability of CTF-Cl was, however, higher than that of CTF-CH_3 (Fig. 3b) [53]. This phenomenon was identical to hydroxylated and hydrogenated graphene nanopores, where the former showed a significantly higher water permeability compared with the latter due to the presence of negative charges on the oxygen atoms of the hydroxyl functional groups [40].

MOFs have been popular for water purification. However, their pore sizes are not suitable for monovalent ion sieving. This issue limited their application only to divalent ion sieving and capacitive deionization [62,63]. Recent studies, however, demonstrated that by stacking 2D MOF, the effective radius of the in-plane nanopore could be reduced, rendering them operational for monovalent ion sieving [55,56]. In one study by Zhou et al. the effect of MOF stacking orientations was investigated on its desalination performance. Although MOF has intrinsic pore sizes of 1.58 nm, unsuitable for monovalent ions blocking, their stacking in multilayer offset fashion can reduce the pore size down to 0.89 nm. Using molecular dynamics simulation, they demonstrated 100% $MgCl_2$ rejection with two orders of magnitude higher water permeance compared with commercial nanofiltration membranes. MOF in fully eclipsed configuration shows higher water permeance, but lower $MgCl_2$ rejection compared with MOF in offset-eclipsed fashion (Fig. 3c and d) [55]. Other classes of MOF with pore sizes of 0.8 nm could also be employed for desalination with water fluxes that are nine times higher than that of MoS_2 or graphene and salt rejection of nearly 90%. The salt rejection could reach approximately 100% with stacking two layers only [56]. Recently, Wang's group demonstrated the application of monolayered MOF for ion sieving. The MOF demonstrated angstrom-sized pores that are suitable for monovalent ion sieving applications. The ~10 nm-thick membrane showed a nearly 100% rejection rate of monovalent ions with water permeability of 0.04 LMHB. Due to parallel π- π interaction of the self-locked membrane, the nanosheets could maintain an interlayer spacing of 6.1 Å, resulting in a stable desalination performance up to 750 h (Fig. 3e–g). This work could be the milestone for future studies of practical MOF membranes for water desalination [57]. Research devotion to the fabrication of 2D MOF's with large lateral sizes could also significantly contribute to these classes of membranes [64].

The family of graphynes could also be promising for water desalination due to their tunable pore sizes relative to their structural configurations [58–61]. Via molecular dynamics simulations, Lin et al. investigated the effect of acetylenic linkage lengths (N) of graphyne on its desalination performance. Upon increasing this linkage number, the pore diameters were also correspondingly increased with the values of 3.8, 5.4, 7.0, and 8.6 Å (Fig. 3h and i). The water permeability was directly proportional to the linkage number, and it could be increased from 2.9×10^{-9} m/Pa/s to 4.5×10^{-9} m/Pa/s. The 100% salt rejection, however, could only be achieved for $N = 3$ (i.e. graphtriyne) with an effective pore diameter of 3.8 Å (Fig. 3j) [59].

4. Stacked membranes

The other alternative to the 2D nanoporous monolayer membranes is the 2D stacked membranes where the solute passes via nanochannels between nanosheets. These membranes can be produced via facile techniques such as vacuum filtration, which eliminates the costly CVD process, rendering them highly cheap and scalable to produce in commercial scales. In addition, stacked membranes benefit from having channels with uniform size and smaller size distribution, parameters that are difficult to control in nanoporous thin membranes [22,23]. This section is mainly devoted to the challenges associated with these types of membranes.

2D materials that are dispersed in liquid environments can be stacked on top of one another using the vacuum filtration technique. However, the stacked nanosheets often re-disperse when tested under actual water purification. The re-dispersion of these nanosheets is referred to as 'swelling' in the membrane community. The swelling often results in membrane disintegration, especially when deployed under cross-flow conditions [20]. Also, the swelling widens the interlayer spacing and results in membrane failure due to the permeation of monovalent ions. It was found that when graphene oxide (GO) membrane is immersed in aqueous solutions, hydration occurs, developing negative charge on GO and resulting

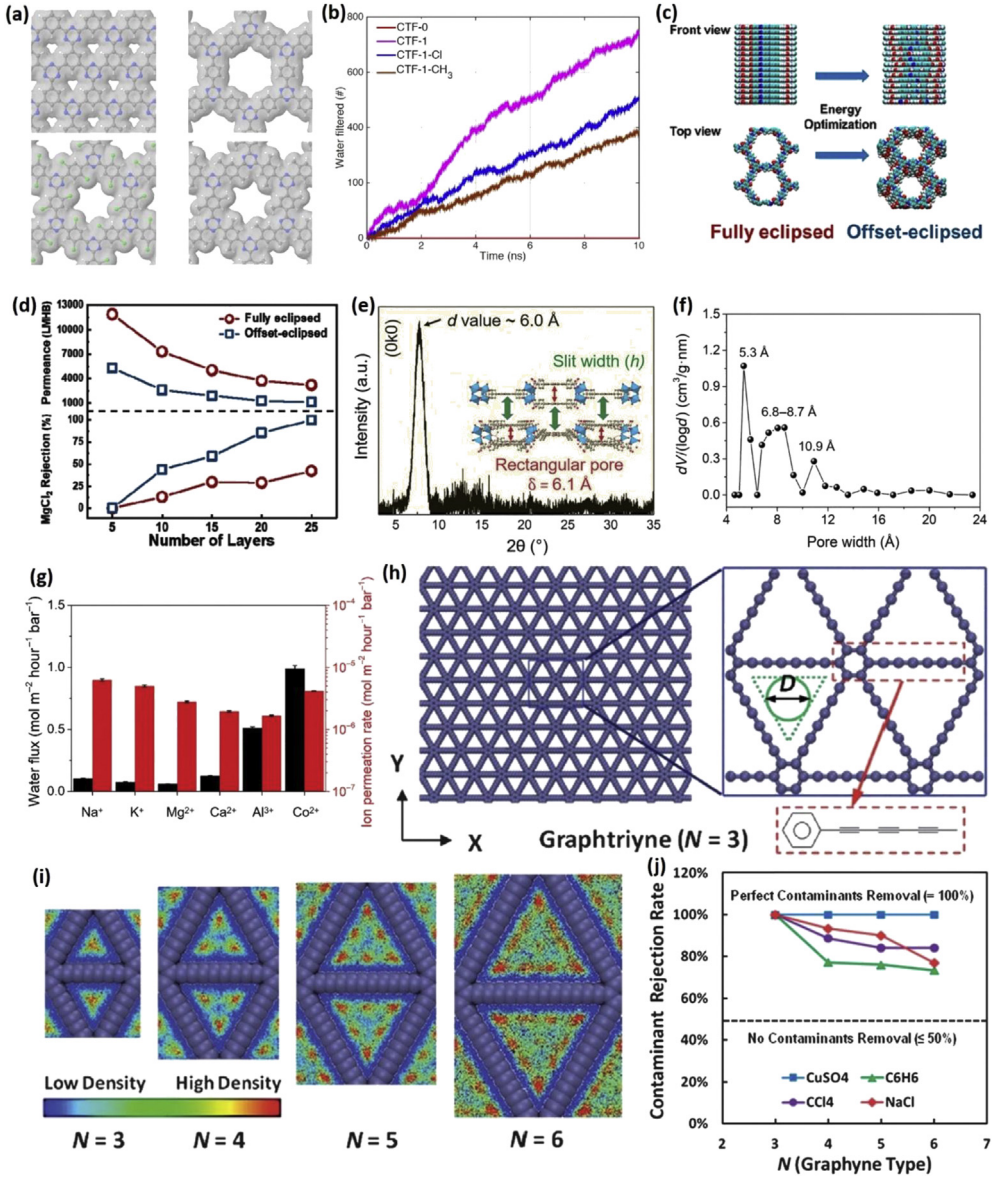

Fig. 3. a) Covalent triazine frameworks (CTFs) with various configurations and chemical functional groups. b) Theoretical simulation of water permeance for CTF. Reproduced with permission [53]. Copyright 2015, Royal Society of Chemistry. c) Multilayer MOF stacked in two styles of fully eclipsed and offset-eclipsed. d) Water permeance and $MgCl_2$ rejection as a function of the number of stacked MOF layers. Reproduced with permission [55]. Copyright 2019, American Chemical Society. Fabrication of ultrathin MOF laminar membrane, depicting e) interlayer spacing, f) pore size distribution, and g) water flux and ion permeation rate. Reproduced with permission [57]. Copyright 2020, American Association for the Advancement of Science (AAAS). h) Atomic structure of the graphyne showing the effective pore diameter of the triangular nanopore. i) Increasing the number of acetylene linkage also increased the effective pore diameter and water density. j) The rejection rate of different contaminants as a function of the acetylene linkage number (*N*). Reproduced with permission [59]. Copyright 2013, Royal Society of Chemistry.

in membrane disintegration due to electrostatic repulsion effects [65]. Finding a way to bind these nanosheets together would ultimately solve this issue. In addition to fixing the interlayers distances, tuning these distances is also consequential for achieving an optimum selectivity/permeability trade-off (i.e. larger interlayer spacing yields higher water permeability but lower salt rejection rate and vice versa) [32].

In this section, our primary focus is to discuss the techniques to tune and fix interlayer spacing of 2D materials yielding robust, stable, and high-performance membranes. The first section elaborates tuning and adjusting interlayer distances without any external component placed within interlayers, while the second section deals with inserting a foreign agent between nanoflakes. In the third section, we discuss anti-swelling 2D materials (i.e. 2D materials that show a diminished degree of swelling when immersed in water) and the effect of salt rejection via Donnan exclusion, making un-necessary the tuning or fixing of interlayer distances.

4.1. Tuning interlayer distances without external component

There are several techniques to tune and fix the interlayer distances of 2D materials, such as controlled-reduction [66–70], dehydroxylation [34], and application of external pressure [31,71,72]. We will review these strategies in this part.

Controlled-reduction of GO could be a promising alternative to tune its interlayer spacing and restrict its swelling [66–70]. Molecular dynamics simulation showed that swelling of GO could be

controlled by optimizing both the flake oxygen content and membrane water content [67]. This study implies that controlled reduction of GO to reduced graphene oxide (rGO), where oxygen functional groups are partially reduced, could yield 2D stacked membranes of various interlayer sizes [68]. The tuning of interlayer distances for the graphene-based membrane can be achieved by the degree of GO reduction from large interlayer spacing for GO (~10 Å) to short interlayer spacing for rGO (~3.5 Å). In one study by Wang's group, complete reduction of GO to rGO was achieved via reducing GO with hydrogen iodide vapor. The free-standing graphene showed excellent water permeability but modest salt rejection, probably due to the loss of polar groups [69]. The controlled reduction of GO could also tailor the size of its nanowrinkles that is an important parameter for mass transportation in laminar membranes [70,73].

Dehydroxylation of chemical bonds, followed by covalent bond formation induced by thermal annealing, could be a simple technique to cross-link the 2D nanosheets together [34]. In fact, the thermal annealing of GO renders possible the partial and controllable reduction of GO with interlaying spacing tunability. However, this comes at the expense of losing polar groups, yielding moderate salt rejection performance [49,74]. The researchers at Wang's team, however, found that the mild annealing of MXene resulted in covalent bonds formation between laminates in a self-cross-linking fashion. This cross-linking occurred via dehydroxylation of MXene sheets where Ti—OH functional groups tend to dehydrate and form stable Ti—O—Ti bonds with fixed interlayer spacing (Fig. 4a). Increasing annealing temperature up to 80 °C resulted in almost 100% salt rejection (Fig. 4b). Interestingly, MXene had an interlayer spacing of ~13 Å, that is much larger than the hydrated radius of sodium (7.5 Å), suggesting surface polarities and hence, Donnan exclusion effect to remain even after annealing. However, the water permeability of this stacked membrane is rather low, which may be due to surface-induced hydrophobicity via dehydration of MXene [34]. This issue promotes scientists to quest for other interlayer tuning techniques without surface chemistry modification of nanosheets such as the application of external pressure [31,71,72].

Scientists expressed different opinions on the impact of external pressure on the performance of stacked membranes. Talyzin et al. suggested that augmenting filtration pressure would increase the permeation of water molecules in the interlayers, resulting in layers expansion [71]. Furthermore, Sun et al. suggested that applied pressure lessened water-ion interaction and yielded lower ionic selectivity [72]. Given these contradicting ideas, Li et al. developed a technique where water molecules did not play a role in compressing GO membranes. Instead, the external pressure was the main factor in the size-controlling of interlayers (Fig. 4c). In this technique, two face-to-face GO membranes were pressed together by two punched steel plates. Multiple ultrafiltration membranes were required to weaken the indentation on GO membrane and also to distribute the external pressure uniformly. The filtration performance was performed under cross-flow filtration, while external pressure was maintained vertically (Fig. 4d). The

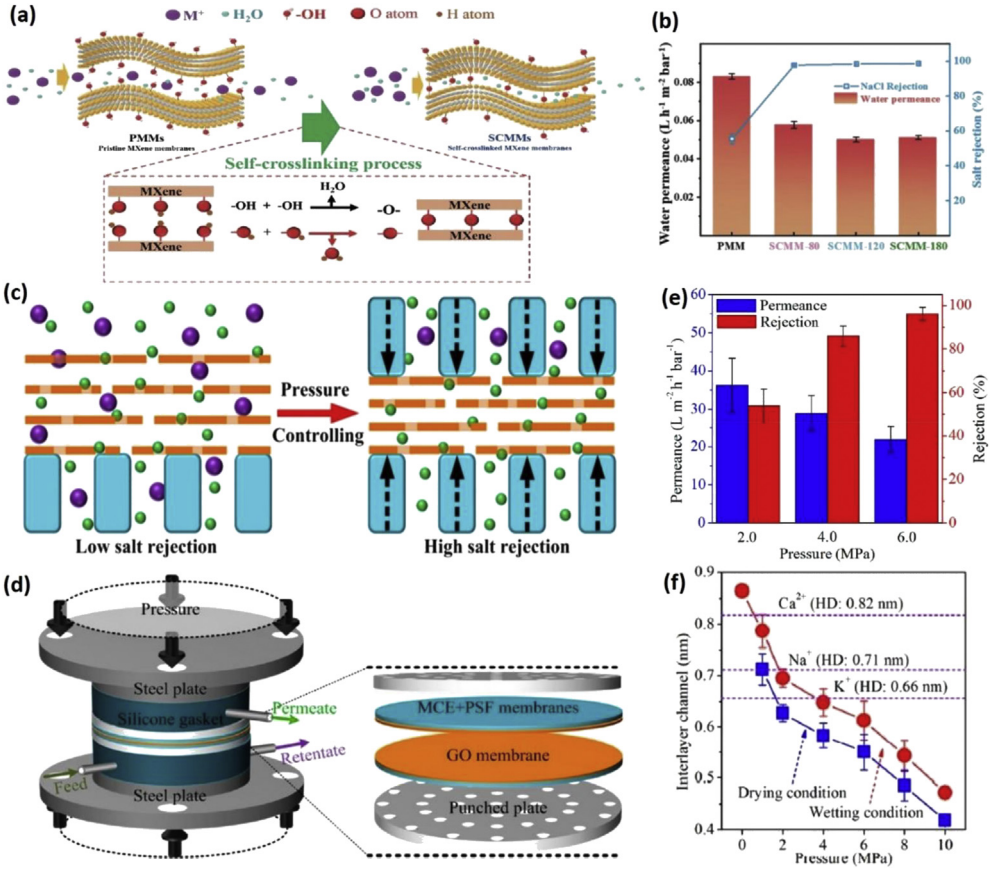

Fig. 4. a) Self cross-linking of MXene via dehydroxylation effect. b) Water permeance and salt rejection for the MXene membrane annealed at different temperatures. Reproduced with permission [34]. Copyright 2019, American Chemical Society. c) Application of external pressure as a technique for regulating interlayer distances. d) The steel plates maintain external pressure, and water is desalinated under cross-flow conduction. e) Water permeability and NaCl rejection as a function of externally applied pressure. f) The interlayer distances can be controlled as a function of applied external pressure. The hydrated radii of cations are also shown for comparison. Reproduced with permission [31]. Copyright 2018, American Chemical Society.

application of 6.0 MPa resulted in the NaCl rejection rate as high as 96.1% with water permeability of 22 LMHB (Fig. 4e). Since the X-ray diffraction (XRD) technique is challenging to characterize GO under external pressure, the interlayer distances of GO were instead obtained by measuring the thickness of GO membrane via a contact thickness gauge with high accuracy. The interlayer distances were successfully tuned relative to the external pressure (Fig. 4f). The XRD tests demonstrated that after removing external pressure, the interlayer distances of GO nanosheets went back to their original value. There are two main drawbacks associated with this technique that is first, the necessity of applying continuous external pressure during filtration and second, the presence of multiple ultrafiltration membranes, which reduces water permeability [31].

4.2. Tuning interlayer distances with an external component

In the above section, tuning of interlayer spacing was achieved intrinsically without the need for a foreign/third-party agent. However, we inferred that the intrinsic functional groups of 2D materials are often not sufficient to develop robust membranes with stable and high performances. Besides, chemical functional groups of 2D materials could also degrade upon self cross-linking. In this section, four methods of interlayer distance tuning and fixing via external components are elaborated. These components can be water molecules [32], metal ions [75–77], monomers [78–84], and polymers [85,86] that we correspondingly discuss in the sections below.

4.2.1. Water molecules

Abraham et al. reported the fabrication of interlayer-tuned GO membrane via relative humidity control, where water molecules intercalated within GO interlayers. The interlayer spacing could be tuned from 6.4 Å to 9.8 Å by controlling the atmospheric humidity. Also, epoxy was applied between GO laminates to prevent swelling of GO layers (Fig. 5a–c). This strategy hindered swelling of GO successfully and yielded NaCl rejection of nearly 97% [32]. Although this study reports a novel membrane with filtration across vertical nanochannels, the fabrication is rather tedious. This is because interlayer distance tuning (i.e. relative humidity control) and interlayer distance fixing (i.e. epoxy binding) are two separate processes. In the following sections, cross-linking via external components will be discussed as a method that not only retains chemical functional groups intact but also adjusts the interlayer distances and also fixes the interlayer spacing, killing three birds with one stone.

4.2.2. Metal ions cross-linkers

Two-dimensional (2D) materials with abundant functional groups such as GO [75,76,87], and MXene [77] can be cross-linked via intercalating metal ions. Modification of GO with small percentages of metal ions such as Mg^{2+} and Ca^{2+} was deemed as an effective strategy to enhance the mechanical stiffness of GO paper significantly. This enhancement was mainly due to electrostatic bonding between metal ions and the carboxylate groups on the edges of GO [87]. To shed further insight into this mechanism, Chen et al. performed a detailed study via hydrated Na^{+} ions. They found the hydrated ion to adsorb via hydrogen bonds at the regions where oxidized groups and aromatic rings co-exist (Fig. 5d–f). Further DFT calculations demonstrated additional pi bonding between hydrated cations and the aromatic rings. Deploying ions of varying hydrated diameter could effectively tune and fix the interlayer distances. The interlayer distances were directly proportional to the hydrated radius of ions in the corresponding Li^{+}> Na^{+}> K^{+} order (Fig. 5g) [75]. Specifically, the hydrated radius is directly proportional to the hydration energy in the ionic shell [8]. GO membranes modified by KCl showed negligible swelling when immersed in different ionic solutions (Fig. 5h).

Amongst the three alkali anions, K^{+} displayed the highest interaction energy and an enormous van der Waals volume (Fig. 5e), demonstrating the fact that potassium ion is the most stable one within GO interlayers. Ghaffar et al. obtained identical results where GO cross-linked by Li^{+} and Na^{+} was not stable in the water while those intercalated by K^{+} were stable [76]. The KCl-controlled membranes demonstrated negligible ion permeation rates for Na^{+}, $Mg^{+,}$ and Ca^{+} ions, with cross-linked GO showing ions rejection rate of more than 99% relative to the pristine GO. However, leaking of ions could partially occur from GO interlayers that are probably due to the weak nature of these hydrogen bondings [75].

In another research by Wang's group, the Al^{3+} could intercalate within the $Ti_3C_2T_x$ MXene membrane, binding the nanosheets together (Fig. 5i). The abundant surface terminations such as = O, −OH, and −F functional groups enable the tuning and controlling of its *d*-spacing. The *d*-spacing could be reduced from ~1.7 nm to ~1.5 nm after Al^{3+} intercalation, and this interlayer spacing remained unaltered upon membrane immersion in water and various salt solutions. Moreover, this strategy proved effective when modified MXene showed a significant reduction in the permeation rate of monovalent and divalent ions compared with unmodified MXene (Fig. 5j). The covalent binding between Al^{3+} and −O functional groups on MXene was so robust that no leaking was observed, with the performance being stable up to 400 h [77].

4.2.3. Monomer cross-linkers

Cross-linking of 2D materials via organic molecules is another effective strategy in tuning and fixing the interlayer distances of laminar membranes. Covalent cross-linking of GO with organic monomers could be achieved via esterification [78], and nucleophilic substitution reaction [79–84] with the latter being more popular due to not deploying highly oxidizing acids. Nucleophilic substitution reaction is usually performed via reactions between aliphatic/aromatic diamines and oxygen-containing groups of 2D materials [79]. The reason for choosing diamine molecules over single amines is that two adjacent nanosheets could react with each amine group, yielding cross-linking between two neighboring nanosheets. In one study by Hung et al. GO was cross-linked by three diamine monomers, namely ethylenediamine (EDA), butylenediamine (BDA) and *p*-phenylenediamine (PDA). The tuning of interlayer distances was directly proportional to the monomer chain length. Furthermore, upon immersion of GO in water, the interlayer stretching was significantly suppressed compared with unmodified GO (Fig. 6a–c). FTIR result demonstrated total attenuation of hydroxyl groups due to condensation and nucleophilic substitution reactions between amines and oxygen-containing groups of GO, forming C–N covalent bonds [79]. Besides the aforementioned symmetric monomers, asymmetric molecules such as polyvinyl alcohol (PVA), *m*-phenylenediamine (MPD), 1,3,5-benzenetricarbonyl (TMC), and the mixture of MPD/TMC could also tune interlayer distances of GO (Fig. 6d) [82].

Apart from the nature of cross-linkers, the ratio between GO and monomers is also very crucial. Hung et al. and Qian et al. utilized an almost identical ratio of GO and diamine monomer and could successfully tune interlayer distances with stable performance for separating water/alcohol mixture [79,80]. To apply this strategy for water desalination, Meng et al. used EDA monomer to cross-link GO but deployed a significantly lower amount of monomer, resulting in low salt rejection performance of 36%. The lack of pressure during the filtration process may be another reason for this unsatisfactory performance [81]. To solve this issue, Hung et al. also utilized a small amount of monomer to GO ratio but instead deployed

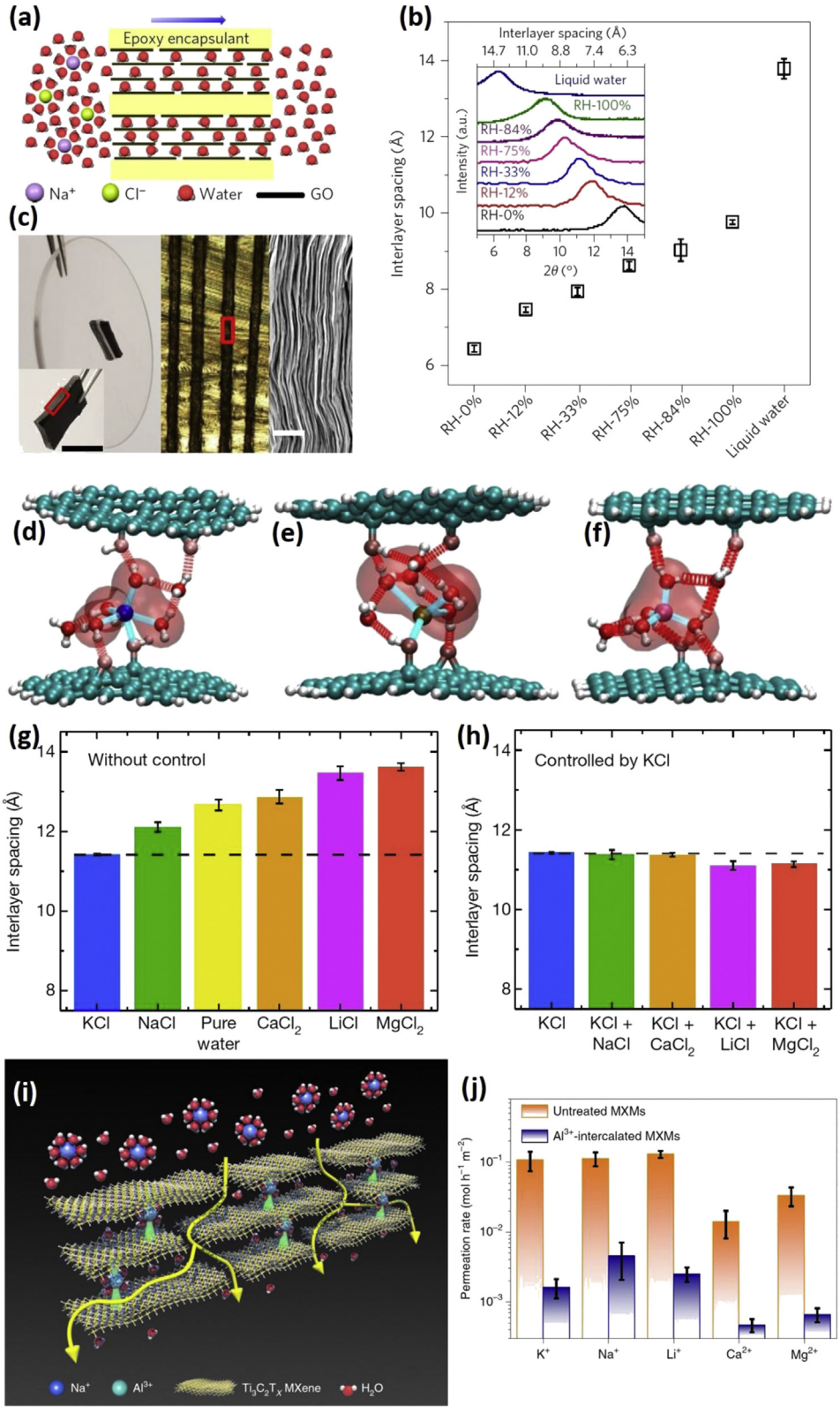

Fig. 5. a) Tuning GO interlayer spacings via inserting a different number of water molecules into GO interlayers by changing the relative humidity atmosphere. Epoxy can be utilized to fix interlayer spacings; b) Interlayer spacing can be adjusted as a function of relative humidity; c) Digital photograph and scanning electron microscopy (SEM) image of the membrane with exposed vertical nanochannels. Reproduced with permission [32]. Copyright 2017, Nature Publishing Group. The most stable geometries of the hydrated cation and GO cluster cross-linked with d) Na^+, e) K^+, and f) Li^+ ions. The transparent red area is the van der Waals volume of the hydration water molecule. g) Interlayer space tuning via different ionic solutions, including pure water. h) The effect of ionic solutions on interlayer spaces of KCl-controlled GO. Every ionic solution is added with an identical amount of KCl to prevent leaking of potassium ions from GO interlayers. Reproduced with permission [75]. Copyright 2017, Nature Publishing Group. i) Inserting Al^{3+} within $Ti_3C_2T_x$ MXene layers as a technique to tune its interlayer distances; j) Ion permeation rate through un-treated and Al^{3+}-intercalated MXene. Reproduced with permission [77]. Copyright 2020, Nature Publishing Group.

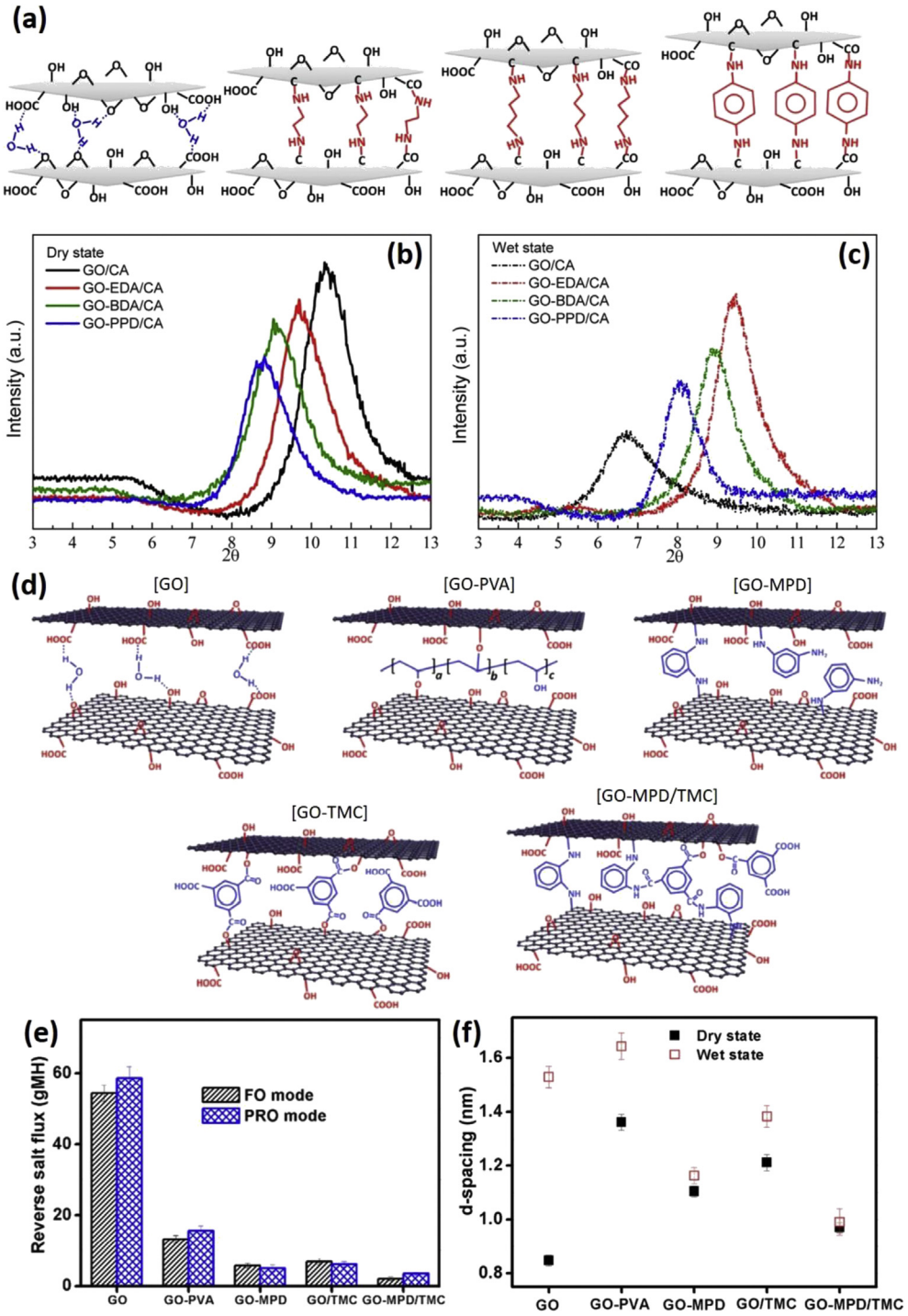

Fig. 6. a) Controlling interlayer distances of GO with symmetric diamine monomers of different chain lengths. Low angle XRD to measure *d*-spacing and interlayer distances of pristine and diamine-functionalized GO in b) dry state, and c) wet state. Diamine functionalization of GO results in a negligible change in *d*-spacing, whereas pristine GO swells significantly. Reproduced with permission [79]. Copyright 2014, American Chemical Society. d) Asymmetric molecules as another strategy to tune interlayer spacing of GO, depicting e) reverse salt flux, and f) *d*-spacing in the wet and dry state. Reproduced with permission [82]. Copyright 2019, Elsevier.

external pressure during membrane fabrication. Consequently, they could adjust interlayer spacing and attained negligible salt permeability of ~1.5 g/h/m^2 that was several orders of magnitude lower compared with pristine GO (Fig. 6e). The smallest possible interlayer distance they could obtain was nearly 10 Å, via MPD/TMC (Fig. 6f) [82]. Surprisingly, the interlayer distances via MPD alone in this work (~11 Å) is 1 Å smaller than that previously reported [79]. This fact demonstrates the importance of GO and monomer ratio to tune interlayer distances, where extensive monomer/GO loading could compress GO nanosheets further. Nicolai et al. theoretically simulated the effect of monomer density on the performance of cross-linked GO and found a very noteworthy relation between monomer density and desalination performance [88]. Hence, utilization of optimum monomer to GO ratio and also the pressure

during filtration are important parameters to consider for effective adjustments and fixation of GO layers for water desalination applications.

We have seen from the previous works that apart from monomer chain length, the ratio of monomer/active material and also the application of external pressure during filtration are essential parameters to consider for these classes of membranes. Although monomer cross-linking strategies can tune and fix the interlayer distances successfully, the *d*-spacings are significantly larger than the hydrated radii of cations. This fact renders the cross-linked monomer membranes, not an option currently for practical water desalination. Applying a smaller chain molecular bridge could probably solve this issue.

However, the lack of nucleophilic sites and oxygen functional groups on other types of 2D materials renders impossible the cross-linking reactions, prompting researchers to quest for alternative cross-linking strategies such as polymers. In-situ polymerization of 2D materials can physically bind and cross-link them together, irrespective of the nature of 2D materials' functional groups. We discuss these classes of cross-linkings in the subsequent section.

4.2.4. Polymer cross-linkers

Several studies reported the incorporation of 2D materials and its composites into polymers, either in the membrane support layer [89,90], or in the active layer [91–94]. In these studies, the incorporation of 2D materials enhanced not only the mechanical rigidity of the polymers but also its hydrophilicity and, consequently, its water permeability [10]. 2D materials can also enhance the salt rejection properties of polyamide membranes [94]. These studies, however, do not report the tuning or fixing of nanosheets. It is by Wang's group where GO is cross-linked and twinned together via free-radical polymerization [85]. What's more, the vacuum filtration pressure could adjust the GO interlayer distances [86]. In their group, they invented a free radical polymerization technique where *N, N′-methylene-bis-acrylamide* (MBA) functions as cross-linker, *N-Isopropylacrylamide* (NIPAM) as monomer followed by *Ammonium Persulfate* (APS) as initiator. These precursors are then in-situ polymerized with GO to develop a highly cross-linked network of GO@polymers (Fig. 7a and b). The prepared membranes demonstrated outstanding antiswelling behaviors with unique desalination capability [85,86]. Altering the vacuum level could tune the thickness as well as the crystallinity of membranes (Fig. 7c and d). Membranes prepared under low vacuum showed amorphous structure, while high vacuum resulted in enhanced crystallinity. Although membranes showed reduced thickness upon increasing vacuum pressure, this did not alter interlayer distances as the changes were merely from amorphous to crystalline, with the latter slightly outperforming the former (Fig. 7e). The cross-linking of GO was so robust that membranes demonstrated anti-compaction properties where the structure remained stable under high pressure, whereas commercial polyamide membrane compacted and displayed reduced water flux (Fig. 7f) [86].

The study mentioned above showed that interlayer fixation could be achieved together with the controllability over membrane crystallinity. The interlayer spacing of the GO was found to be ~1 nm under an applied pressure of 0.1 MPa [86]. The same group also prepared GO@polymer composite via the identical free radical polymerization technique but varied polymer precursors ratio. The spin-coated membrane achieved an interlayer spacing of 0.47 nm instead [85]. These different values may arise due to the varying amount of polymer precursors used. This mechanism, however, is not thoroughly investigated in these works and demands further studies. Hence, to tune the interlayer spacing of stacked sheets via polymer chains, the degree of polymerization and also the applied pressure need consideration.

4.2.5. Hybrids with inorganic materials

The interlayer spacing of 2D materials can be also controlled via developing hybrid nanostructures with inorganic materials [66,95,96]. In one study, graphene oxide quantum dots (GQD) could successfully cross-link GO sheets. Abundant hydroxyl and carboxyl groups in GQD enabled the stitching of GO sheets via an esterification reaction. The cross-linked GO membrane demonstrated a reduced interlayer spacing of 6.1 Å and an enhanced Na_2 SO_4 rejection rate from 88% to 98% [95]. In another study by Ma's group, cationic Co–Al and Mg–Al layered double hydroxide (LDH) nanosheets stabilized the anionic GO nanosheets via the electrostatic face-to-face self-assembly process. The LDH/GO superlattice structure could successfully prevent the swelling of GO in aqueous media. Furthermore, their vacuum-filtered free-standing membrane depicted a relative selectivity of as high as 30 between monovalent and trivalent cations. This performance is attributed to the molecular-level self-assembly of the nanosheets and also the positive electrostatic charge on LDH nanosheets [96].

4.3. The issues beyond tuning interlayer distances

Besides the importance of tuning interlayer distances, we need to consider four significant issues for realizing practical applications of stacked membranes. These issues are first, the 2D materials with antiswelling properties [97–99], the role of surface chemistry in 2D materials [33,100], the function of a separate salt-blocking layer on top of stacked membranes [35,97], and lastly the binding between 2D materials and the substrate [35,83,101–103].

It is noteworthy to mention some of the 2D stacked membranes that are developed, such as MoS_2, demonstrates some intrinsic antiswelling properties. More research devotion to these types of materials could greatly simplify the membrane fabrication process and increase their filtration stabilities. Interestingly, stacked MoS_2 nanoflakes demonstrated an identical interlayer spacing of (~0.65 nm) with that of the bulk MoS_2. This fact suggests that the electrostatic field on the surface of MoS_2 nanosheets is not high enough, probably rendering the re-stacking of nanosheets with interlayer spacing down to the size of its bulk structure. Moreover, due to these electrostatic field deficiencies and also the lack of hydrophilicity on the surface layers, fewer water molecules will be intercalated within the nanosheets, and hence swelling can be prevented [97,98]. For the multilayer MoS_2 stacked membrane that is fabricated via CVD, this spacing was suitable to permeate water molecules and reject NaCl with 98% rates up to 24 h [98]. However, for the vacuum-filter deposited membrane that was fabricated via solvent exfoliation of MoS_2, the rejection of NaCl was not satisfactory unless functionalized by organic dyes [97]. On the other hand, the MoS_2 membrane prepared via lithium exfoliation technique yielded negligible NaCl permeation on the order of 10^{-12} m^{-2} s^{-1} [99]. These studies emphasize that although some materials may demonstrate anti-swelling properties, the role of the functional group and surface chemistry cannot be neglected. Hence, membranes with anti-swelling properties but without proper surface polarity are still un-operational [100].

To elucidate the role of surface chemistry, Song et al. incorporated pyridinic nitrogen sites on GO as polar groups to reject salts via the Donnan effect. Increasing the nitrogen doping amount impeded the permeability of ions, specifically the monovalent K^+ and Na^+ (Fig. 8a and b). Interestingly, they observed no correlation for other nitrogen-bonding configurations such as pyrrolic-N and graphitic-N. This is due to the strong polarization effects and high adsorption energy of pyridinic nitrogen, rendering possible the significant electrostatic interactions with ions [33]. In another work, Ries et al. grafted different functional groups with varying degrees of polarity on MoS_2 nanosheets. They found that a small

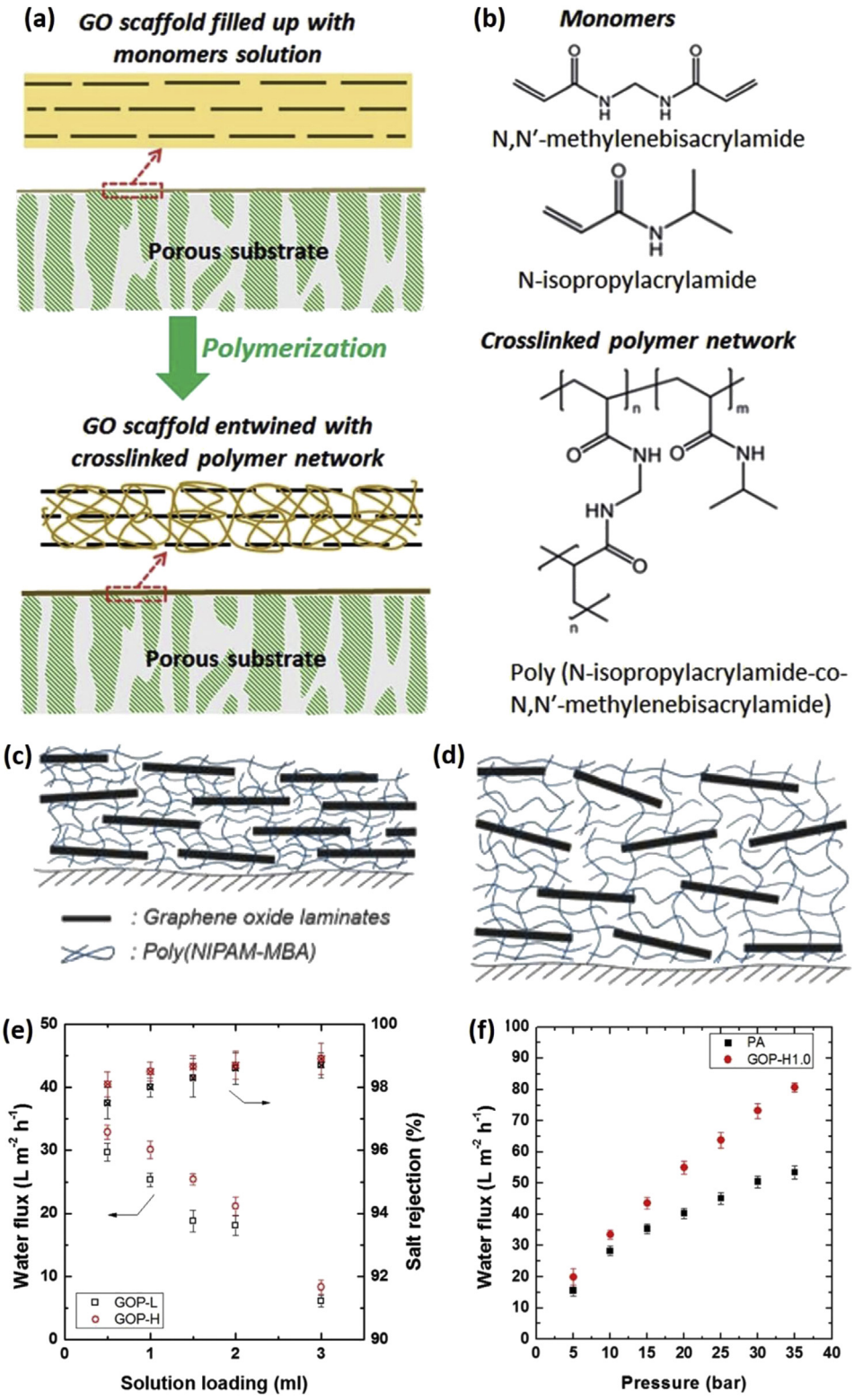

Fig. 7. a) Schematic for in-situ free-radical polymerization of GO. b) Molecular structures of monomers MBA and NIPAM. Reproduced with permission [85]. Copyright 2017, Royal Society of Chemistry. Fabrication of GO@polymer cross-linked membrane where the vacuum filtration pressure can tune the thickness and crystallinity of the membrane. The schematic of membranes prepared under c) high vacuum pressure and d) low vacuum pressure. e) Water flux and salt rejection properties of GO@polymer membrane as a function of solution loading where GOP-L and GOP-H show membranes developed under low and high vacuum, respectively. The GOP-L shows lower membrane performance due to its amorphous structure. f) Comparison of water flux for GO-polymer membrane (GOP-H1.0) vs. commercial polyamide (PA) membrane as a function of applied pressure. Reproduced with permission [86]. Copyright 2018, Elsevier.

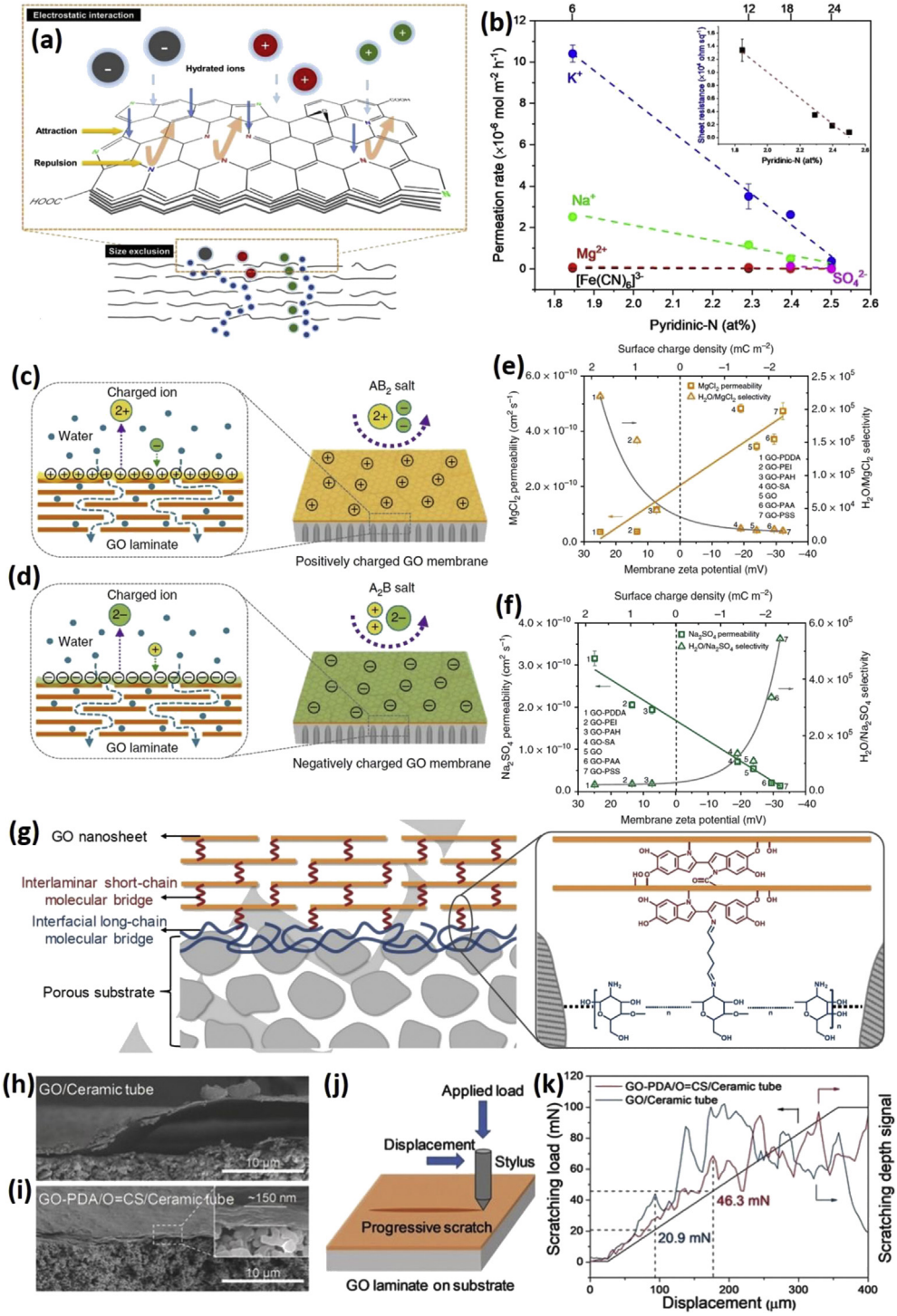

Fig. 8. a) Ion sieving via the combined effect of electrostatic repulsion and size exclusion. b) The relationship between pyridinic-N content of GO and permeation rate for various ions. Reproduced with permission [33]. Copyright 2018, American Chemical Society. Depositing positively and negatively charged polyelectrolyte on GO to repel high-valent c) cations and d) anions. Permeability of e) $MgCl_2$ and f) Na_2SO_4 as a function of membrane zeta potential. Reproduced with permission [35]. Copyright 2019, Nature Publishing Group. g) The interfacial long-chain molecular bridge as a strategy to chemically bind GO with its substrate. The long-chain bridge (shown in blue) bind with amine-functionalized GO via O═CS groups. h) SEM image of GO and unmodified ceramic tube and i) modified with long-chain bridges. Molecular bridges prevent the peeling-off of GO from the substrate and also reduces the air gap between GO and its substrate, representative of its intimate contact. j) The setup for the AFM nanoscratch technique. k) Results of nanoscratch measurements with molecular bridges outperforming unmodified membrane in terms of the value of the critical load. Reproduced with permission [83]. Copyright 2019, John Wiley and Sons.

degree of functionalization can maintain salt rejection rates, but it can dramatically enhance water permeability due to interlayer expansion [100]. These two studies demonstrate that doping or chemical functionalization could optimize the surface polarity of 2D materials, making them useful for water desalination.

Apart from modifying the surface chemistry of nanosheets, functionalizing the top surface layers in the stacked membrane, via coating separate ionic or organic molecules, could also effectually reject salts via the Donnan effect [35,97]. In one study by Jin's group, the coating of electrostatically charged polymers on top of GO could dramatically enhance its $MgCl_2$ rejection rate by a factor of more than two times, reaching 96%. Besides, this additional layer did not reduce water permeability due to its hydrophilic nature. The surface charge of GO could be tuned from highly positive via polydiallyl dimethyl ammonium (PDDA) to highly negative via polystyrene sulfonate (PSS). The permeability of $MgCl_2$ increased upon altering membrane surface charge from positive to negative, while Na_2SO_4 displayed a reverse trend. This revealed that high valent anions $(SO_4)^{2-}$ and cations $(Mg)^{2+}$ are repelled by negatively charged and positively charged GO, respectively (Fig. 8c–f). For NaCl, however, the transport behavior remained approximately unchanged due to the electrostatic balance between monovalent co-ions and counter-ions [35].

Last, it is essential to state the effect of substrate chemical functional groups on the binding properties of the 2D stacked materials with its underlying support. Treating beforehand the substrate in organic [83,101,102], or alkaline media [35,103] could form abundant functional groups, yielding an enhanced interfacial adhesion between the substrate and 2D materials. Researchers at Jin's group, found that treating beforehand the ceramic tube in aldehyde-modified chitosan could develop plenty of O═CS groups that are beneficial for chemical binding with amine-functionalized GO. The AFM nanoscratch technique was utilized to measure the interfacial binding force of GO with the substrate. The membrane that had been treated beforehand showed the critical load at failure of 46.3 mN that is more than twice compared with the unmodified membrane (Fig. 8g–k) [83]. Their group also found that GO deposited on polyacrylonitrile (PAN) develops small cracks under cross-flow filtration. However, after treating PAN in NaOH, no detachment was observed. This was attributed to the abundant oxygen functional groups on the surface of PAN after hydrolysis that could bind well with GO [103].

These studies suggest that the Donnan exclusion effect (where electrostatic fields are either on the surface of nanosheets or as a separately coated layer on the top surface of membranes) can be the principal filtration mechanism both for swelling and anti-swelling materials. Furthermore, membrane swelling, water permeability, and salt rejection rates are proportional to the surface polarities of 2D stacked membranes. Hence, the electrostatic charges on nanosheets that yield these trade-offs need to be delicately optimized and taken into consideration. Last, treatment beforehand of the substrate to form chemical bonding with 2D materials and avoidance of its detachment are necessary for long-term and steady operation.

5. Summary and outlook

We have reviewed the progress and challenges of developing 2D materials for membrane-based water desalination. Water desalination and ion sieving across 2D materials can be achieved either via physical size exclusion or electrostatic Donnan exclusion effect. Two classes of membranes can be developed based on 2D materials, which are monolayers with in-plane nanopores or the stacked nanosheets with nanochannels in between.

Water desalination can be performed via monolayers with the in-plane externally drilled nanopore. Several factors such as defects, pore sizes, and pore surface chemistry, need to be considered. Drilling an external pore on the surface of monolayers was traditionally done via the ion bombardment technique. However, new oxygen plasma etching has shown promise on graphene as it produces significantly higher water flux due to surface chemistry modifications, together with size tunability features. Due to the atomic layer thickness of these membranes, the mechanical properties can be improved via incorporation with nanowire backbone such as carbon nanotubes. Several 2D materials, including covalent triazine frameworks, MOFs, and graphynes, have subnanometer pore sizes for water desalination, where altering the phases or stacking configurations could optimize their pore sizes.

Compared with nanoporous monolayer membranes, 2D stacked membranes have better scalability and mechanical properties, but often re-disperse in liquid media and are thus required to be stabilized and fixed by some techniques. The interlayer distances of 2D stacked membranes can be optimized via controlled reduction, dehydroxylation, and changing external pressure. Certain materials and applications demand to insert an external component in between the interlayers to cross-link and bind adjacent layers together. These components can be water molecules, metal ions, and organic monomers. The combined strategy of vacuum pressure and polymers can also be utilized to tune and fix interlayers, respectively. Apart from tuning and adjusting interlayer distances, some critical parameters demands further investigations. These include salt rejection via Donnan exclusion by modifying the surface polarities of the stacked nanosheets, and the chemical treatment of the substrate to increase its binding force with the stacked 2D materials.

Despite the numerous progress achieved in this field, several areas of research demand additional attention. First, regarding nanoporous membranes: although researchers have performed extensive theoretical and experimental studies on ions sieving via graphene nanopores, other types of 2D materials need to be explored. Furthermore, attention should be paid to the nature of pore chemistry and pore fabrication technique. Second, considering stacked membranes, apart from developing innovative and scalable methods to tune and fix interlayer distances of 2D nanosheets, we should consider the development of 2D materials with anti-swelling properties with interlayer sizes below hydration radius of cations. This achievement could eliminate the tedious interlayer tuning process, which could greatly simplify the fabrication process and also enhance the stability of desalination membranes. Self-assembled 2D superlattices are also other promising types of stacked membranes. In these membranes, the stability and overall performance can be improved due to the synergy between the two heterogeneous nanoflakes at the molecular level [96]. Third, the combination of nanoporous and stacked membranes with in-plane nanopores is worth to be comprehensively investigated. In this scenario, water permeates not only via the nanochannels of 2D stacked membranes but also through the in-plane pores of the nanosheets. Recent studies on 2D MOF with angstrom-sized pores could herald a promising future for lamellar nanoporous membranes [57]. Last, altering the surface chemistry of 2D materials could streamline the membrane fabrication process since Donnan electrostatic exclusion effect comes into play instead of the physical size exclusion [35,97]. This technique could be applied either on a diverse range of antiswelling or swelling 2D materials with various

interlayer sizes. Tackling the multiple challenges faced in 2D membranes could achieve next generation of practical high-performance water desalination membranes.

Declaration of competing interest

The authors declare that they have no known competing financial interests or personal relationships that could have appeared to influence the work reported in this paper.

Acknowledgments

We acknowledge the financial support by the Australian Research Council (ARC) through the ARC Discovery projects (DP170100436 and DP200101249).

References

[1] A. Lee, J.W. Elam, S.B. Darling, Membrane materials for water purification: design, development, and application, Environ. Sci.: Water Res. Technol. 2 (2016) 17–42.
[2] S. Dutta, S.-Y. Huang, C. Chen, J.E. Chen, Z.A. Alothman, Y. Yamauchi, C.-H. Hou, K.C.-W. Wu, Cellulose framework directed construction of hierarchically porous carbons offering high-performance capacitive deionization of brackish water, ACS Sustain. Chem. Eng. 4 (2016) 1885–1893.
[3] T. Oki, S. Kanae, Global hydrological cycles and world water resources, Science 313 (2006) 1068–1072.
[4] M. Wang, X. Xu, J. Tang, S. Hou, M.S.A. Hossain, L. Pan, Y. Yamauchi, High performance capacitive deionization electrodes based on ultrathin nitrogen-doped carbon/graphene nano-sandwiches, Chem. Commun. 53 (2017) 10784–10787.
[5] X. Xu, A.E. Allah, C. Wang, H. Tan, A.A. Farghali, M.H. Khedr, V. Malgras, T. Yang, Y. Yamauchi, Capacitive deionization using nitrogen-doped mesostructured carbons for highly efficient brackish water desalination, Chem. Eng. J. 362 (2019) 887–896.
[6] J.R. Werber, C.O. Osuji, M. Elimelech, Materials for next-generation desalination and water purification membranes, Nat. Rev. Mater. 1 (2016) 1–15.
[7] J.F. Anthoni, The chemical composition of seawater, Magnesium 2701 (2006) 96–9062.
[8] B. Tansel, Significance of thermodynamic and physical characteristics on permeation of ions during membrane separation: hydrated radius, hydration free energy and viscous effects, Separ. Purif. Technol. 86 (2012) 119–126.
[9] R. Epsztein, R.M. DuChanois, C.L. Ritt, A. Noy, M. Elimelech, Towards single-species selectivity of membranes with subnanometre pores, Nat. Nanotechnol. 15 (2020) 426–436.
[10] W.J. Koros, C. Zhang, Materials for next-generation molecularly selective synthetic membranes, Nat. Mater. 16 (2017) 289–297.
[11] J.R. Werber, A. Deshmukh, M. Elimelech, The critical need for increased selectivity, not increased water permeability, for desalination membranes, Environ. Sci. Technol. Lett. 3 (2016) 112–120.
[12] P. Marchetti, M.F. Jimenez Solomon, G. Szekely, A.G. Livingston, Molecular separation with organic solvent nanofiltration: a critical review, Chem. Rev. 114 (2014) 10735–10806.
[13] Y. Han, Z. Xu, C. Gao, Ultrathin graphene nanofiltration membrane for water purification, Adv. Funct. Mater. 23 (2013) 3693–3700.
[14] L. Huang, M. Zhang, C. Li, G. Shi, Graphene-based membranes for molecular separation, J. Phys. Chem. Lett. 6 (2015) 2806–2815.
[15] D.H. Seo, S. Pineda, Y.C. Woo, M. Xie, A.T. Murdock, E.Y. Ang, Y. Jiao, M.J. Park, S.I. Lim, M. Lawn, Anti-fouling graphene-based membranes for effective water desalination, Nat. Commun. 9 (2018) 1–12.
[16] K.M. Gupta, K. Zhang, J. Jiang, Water desalination through zeolitic imidazolate framework membranes: significant role of functional groups, Langmuir 31 (2015) 13230–13237.
[17] Z. Hu, Y. Chen, J. Jiang, Zeolitic imidazolate framework-8 as a reverse osmosis membrane for water desalination: insight from molecular simulation, J. Chem. Phys. 134 (2011), 134705.
[18] B. Corry, Designing carbon nanotube membranes for efficient water desalination, J. Phys. Chem. B 112 (2008) 1427–1434.
[19] Z. Zheng, R. Grünker, X. Feng, Synthetic two-dimensional materials: a new paradigm of membranes for ultimate separation, Adv. Mater. 28 (2016) 6529–6545.
[20] B. Mi, Graphene oxide membranes for ionic and molecular sieving, Science 343 (2014) 740–742.
[21] Y. You, V. Sahajwalla, M. Yoshimura, R.K. Joshi, Graphene and graphene oxide for desalination, Nanoscale 8 (2016) 117–119.
[22] Y. Kang, Y. Xia, H. Wang, X. Zhang, 2D laminar membranes for selective water and ion transport, Adv. Funct. Mater. 29 (2019) 1902014.
[23] S. Kim, H. Wang, Y.M. Lee, 2D nanosheets and their composite membranes for water, gas, and ion separation, Angew. Chem. 131 (2019) 17674–17689.
[24] R. Nair, H. Wu, P. Jayaram, I. Grigorieva, A. Geim, Unimpeded permeation of water through helium-leak–tight graphene-based membranes, Science 335 (2012) 442–444.
[25] R. Joshi, P. Carbone, F.C. Wang, V.G. Kravets, Y. Su, I.V. Grigorieva, H. Wu, A.K. Geim, R.R. Nair, Precise and ultrafast molecular sieving through graphene oxide membranes, Science 343 (2014) 752–754.
[26] S. Dervin, D.D. Dionysiou, S.C. Pillai, 2D nanostructures for water purification: graphene and beyond, Nanoscale 8 (2016) 15115–15131.
[27] G. Liu, W. Jin, N. Xu, Two-dimensional-material membranes: a new family of high-performance separation membranes, Angew. Chem. Int. Ed. 55 (2016) 13384–13397.
[28] G. Liu, W. Jin, N. Xu, Graphene-based membranes, Chem. Soc. Rev. 44 (2015) 5016–5030.
[29] P. Liu, J. Hou, Y. Zhang, L. Li, L. Xiaoquan, Z. Tang, Two-dimensional material membranes for critical separations, Inorg. Chem. Front. 7 (2020) 2560–2581.
[30] S.P. Surwade, S.N. Smirnov, I.V. Vlassiouk, R.R. Unocic, G.M. Veith, S. Dai, S.M. Mahurin, Water desalination using nanoporous single-layer graphene, Nat. Nanotechnol. 10 (2015) 459.
[31] W. Li, W. Wu, Z. Li, Controlling interlayer spacing of graphene oxide membranes by external pressure regulation, ACS Nano 12 (2018) 9309–9317.
[32] J. Abraham, K.S. Vasu, C.D. Williams, K. Gopinadhan, Y. Su, C.T. Cherian, J. Dix, E. Prestat, S.J. Haigh, I.V. Grigorieva, Tunable sieving of ions using graphene oxide membranes, Nat. Nanotechnol. 12 (2017) 546.
[33] J.-h. Song, H.-W. Yu, M.-H. Ham, I.S. Kim, Tunable ion sieving of graphene membranes through the control of nitrogen-bonding configuration, Nano Lett. 18 (2018) 5506–5513.
[34] Z. Lu, Y. Wei, J. Deng, L. Ding, Z.-K. Li, H. Wang, Self-Crosslinked MXene ($Ti_3C_2T_x$) membranes with good antiswelling property for monovalent metal ion exclusion, ACS Nano 13 (2019) 10535–10544.
[35] M. Zhang, K. Guan, Y. Ji, G. Liu, W. Jin, N. Xu, Controllable ion transport by surface-charged graphene oxide membrane, Nat. Commun. 10 (2019) 1253.
[36] G.-R. Xu, J.-M. Xu, H.-C. Su, X.-Y. Liu, H.-L. Zhao, H.-J. Feng, R. Das, Two-dimensional (2D) nanoporous membranes with sub-nanopores in reverse osmosis desalination: latest developments and future directions, Desalination 451 (2019) 18–34.
[37] A. Boretti, S. Al-Zubaidy, M. Vaclavikova, M. Al-Abri, S. Castelletto, S. Mikhalovsky, Outlook for graphene-based desalination membranes, npj Clean Water 1 (2018) 1–11.
[38] T. Jain, B.C. Rasera, R.J.S. Guerrero, M.S. Boutilier, S.C. O'hern, J.-C. Idrobo, R. Karnik, Heterogeneous sub-continuum ionic transport in statistically isolated graphene nanopores, Nat. Nanotechnol. 10 (2015) 1053.
[39] S.C. O'Hern, D. Jang, S. Bose, J.-C. Idrobo, Y. Song, T. Laoui, J. Kong, R. Karnik, Nanofiltration across defect-sealed nanoporous monolayer graphene, Nano Lett. 15 (2015) 3254–3260.
[40] D. Cohen-Tanugi, J.C. Grossman, Water desalination across nanoporous graphene, Nano Lett. 12 (2012) 3602–3608.
[41] M. Heiranian, A.B. Farimani, N.R. Aluru, Water desalination with a single-layer MoS_2 nanopore, Nat. Commun. 6 (2015) 1–6.
[42] G.A. Ferrari, A.B. de Oliveira, I. Silvestre, M.J. Matos, R.J. Batista, T.F. Fernandes, L.M. Meireles, G.S. Eliel, H. Chacham, B.R. Neves, Apparent softening of wet graphene membranes on a microfluidic platform, ACS Nano 12 (2018) 4312–4320.
[43] Y. Yang, X. Yang, L. Liang, Y. Gao, H. Cheng, X. Li, M. Zou, R. Ma, Q. Yuan, X. Duan, Large-area graphene-nanomesh/carbon-nanotube hybrid membranes for ionic and molecular nanofiltration, Science 364 (2019) 1057–1062.
[44] M.S. Dresselhaus, A. Jorio, M. Hofmann, G. Dresselhaus, R. Saito, Perspectives on carbon nanotubes and graphene Raman spectroscopy, Nano Lett. 10 (2010) 751–758.
[45] M.E. Suk, N.R. Aluru, Ion transport in sub-5-nm graphene nanopores, J. Chem. Phys. 140 (2014), 084707.
[46] P. Masih Das, J.P. Thiruraman, Y.-C. Chou, G. Danda, M. Drndic, Centimeter-scale nanoporous 2D membranes and ion transport: porous MoS_2 monolayers in a few-layer matrix, Nano Lett. 19 (2018) 392–399.
[47] J. Feng, K. Liu, M. Graf, M. Lihter, R.D. Bulushev, D. Dumcenco, D.T. Alexander, D. Krasnozhon, T. Vuletic, A. Kis, Electrochemical reaction in single layer MoS_2: nanopores opened atom by atom, Nano Lett. 15 (2015) 3431–3438.
[48] Y. Yamada, K. Murota, R. Fujita, J. Kim, A. Watanabe, M. Nakamura, S. Sato, K. Hata, P. Ercius, J. Ciston, Subnanometer vacancy defects introduced on graphene by oxygen gas, J. Am. Chem. Soc. 136 (2014) 2232–2235.
[49] Y. Li, W. Zhao, M. Weyland, S. Yuan, Y. Xia, H. Liu, M. Jian, J. Yang, C.D. Easton, C. Selomulya, Thermally reduced nanoporous graphene oxide membrane for desalination, Environ. Sci. Technol. 53 (2019) 8314–8323.
[50] M.A. Shannon, P.W. Bohn, M. Elimelech, J.G. Georgiadis, B.J. Marinas, A.M. Mayes, Science and technology for water purification in the coming decades, Nature 452 (2008) 301–310.
[51] J.P. Thiruraman, K. Fujisawa, G. Danda, P.M. Das, T. Zhang, A. Bolotsky, N. Perea-López, A. Nicolaï, P. Senet, M. Terrones, Angstrom-size defect creation and ionic transport through pores in single-layer MoS_2, Nano Lett. 18 (2018) 1651–1659.
[52] G.H. Ryu, A. France-Lanord, Y. Wen, S. Zhou, J.C. Grossman, J.H. Warner, Atomic structure and dynamics of self-limiting sub-nanometer pores in monolayer WS_2, ACS Nano 12 (2018) 11638–11647.
[53] L.-C. Lin, J. Choi, J.C. Grossman, Two-dimensional covalent triazine framework as an ultrathin-film nanoporous membrane for desalination, Chem. Commun. 51 (2015) 14921–14924.

[54] Y. Yang, W. Li, H. Zhou, X. Zhang, M. Zhao, Tunable C2N membrane for high efficient water desalination, Sci. Rep. 6 (2016) 29218.
[55] W. Zhou, M. Wei, X. Zhang, F. Xu, Y. Wang, Fast desalination by multilayered covalent organic framework (COF) nanosheets, ACS Appl. Mater. Interfaces 11 (2019) 16847–16854.
[56] Z. Cao, V. Liu, A. Barati Farimani, Water desalination with two-dimensional metal–organic framework membranes, Nano Lett. 19 (2019) 8638–8643.
[57] M. Jian, R. Qiu, Y. Xia, J. Lu, Y. Chen, Q. Gu, R. Liu, C. Hu, J. Qu, H. Wang, Ultrathin water-stable metal-organic framework membranes for ion separation, Sci. Adv. 6 (2020), e3998.
[58] Y. Li, L. Xu, H. Liu, Y. Li, Graphdiyne and graphyne: from theoretical predictions to practical construction, Chem. Soc. Rev. 43 (2014) 2572–2586.
[59] S. Lin, M.J. Buehler, Mechanics and molecular filtration performance of graphyne nanoweb membranes for selective water purification, Nanoscale 5 (2013) 11801–11807.
[60] J. Kou, X. Zhou, H. Lu, F. Wu, J. Fan, Graphyne as the membrane for water desalination, Nanoscale 6 (2014) 1865–1870.
[61] M. Xue, H. Qiu, W. Guo, Exceptionally fast water desalination at complete salt rejection by pristine graphyne monolayers, Nanotechnology 24 (2013) 505720.
[62] X. Liu, N.K. Demir, Z. Wu, K. Li, Highly water-stable zirconium metal–organic framework UiO-66 membranes supported on alumina hollow fibers for desalination, J. Am. Chem. Soc. 137 (2015) 6999–7002.
[63] Z. Wang, X. Xu, J. Kim, V. Malgras, R. Mo, C. Li, Y. Lin, H. Tan, J. Tang, L. Pan, Nanoarchitectured metal–organic framework/polypyrrole hybrids for brackish water desalination using capacitive deionization, Mater. Horiz. 6 (2019) 1433–1437.
[64] M. Jian, H. Liu, T. Williams, J. Ma, H. Wang, X. Zhang, Temperature-induced oriented growth of large area, few-layer 2D metal–organic framework nanosheets, Chem. Commun. 53 (2017) 13161–13164.
[65] C.-N. Yeh, K. Raidongia, J. Shao, Q.-H. Yang, J. Huang, On the origin of the stability of graphene oxide membranes in water, Nat. Chem. 7 (2015) 166.
[66] P. Sun, Q. Chen, X. Li, H. Liu, K. Wang, M. Zhong, J. Wei, D. Wu, R. Ma, T. Sasaki, Highly efficient quasi-static water desalination using monolayer graphene oxide/titania hybrid laminates, NPG Asia Mater. 7 (2015) e162.
[67] C.D. Williams, P. Carbone, F.R. Siperstein, In silico design and characterization of graphene oxide membranes with variable water content and flake oxygen content, ACS Nano 13 (2019) 2995–3004.
[68] G. Shi, Q. Meng, Z. Zhao, H.-C. Kuan, A. Michelmore, J. Ma, Facile fabrication of graphene membranes with readily tunable structures, ACS Appl. Mater. Interfaces 7 (2015) 13745–13757.
[69] H. Liu, H. Wang, X. Zhang, Facile fabrication of freestanding ultrathin reduced graphene oxide membranes for water purification, Adv. Mater. 27 (2015) 249–254.
[70] S. Yuan, Y. Li, Y. Xia, Y. Kang, J. Yang, M.H. Uddin, H. Liu, C. Selomulya, X. Zhang, Minimizing non-selective nanowrinkles of reduced graphene oxide laminar membranes for enhanced NaCl rejection, Environ. Sci. Technol. Lett. 7 (2020) 273–279.
[71] A.V. Talyzin, V.L. Solozhenko, O.O. Kurakevych, T. Szabó, I. Dékány, A. Kurnosov, V. Dmitriev, Colossal pressure-induced lattice expansion of graphite oxide in the presence of water, Angew. Chem. Int. Ed. 47 (2008) 8268–8271.
[72] P. Sun, R. Ma, H. Deng, Z. Song, Z. Zhen, K. Wang, T. Sasaki, Z. Xu, H. Zhu, Intrinsic high water/ion selectivity of graphene oxide lamellar membranes in concentration gradient-driven diffusion, Chem. Sci. 7 (2016) 6988–6994.
[73] Y. Kang, R. Qiu, M. Jian, P. Wang, Y. Xia, B. Motevalli, W. Zhao, Z. Tian, J.Z. Liu, H. Wang, The role of nanowrinkles in mass transport across graphene-based membranes, Adv. Funct. Mater. (2020), 2003159.
[74] L. Huang, Y. Li, Q. Zhou, W. Yuan, G. Shi, Graphene oxide membranes with tunable semipermeability in organic solvents, Adv. Mater. 27 (2015) 3797–3802.
[75] L. Chen, G. Shi, J. Shen, B. Peng, B. Zhang, Y. Wang, F. Bian, J. Wang, D. Li, Z. Qian, Ion sieving in graphene oxide membranes via cationic control of interlayer spacing, Nature 550 (2017) 380–383.
[76] A. Ghaffar, L. Zhang, X. Zhu, B. Chen, Scalable graphene oxide membranes with tunable water channels and stability for ion rejection, Environ. Sci.: Nano 6 (2019) 903–915.
[77] L. Ding, L. Li, Y. Liu, Y. Wu, Z. Lu, J. Deng, Y. Wei, J. Caro, H. Wang, Effective ion sieving with $Ti_3C_2T_x$ MXene membranes for production of drinking water from seawater, Nature Sustain. 3 (2020) 296–302.
[78] Z. Jia, Y. Wang, Covalently crosslinked graphene oxide membranes by esterification reactions for ions separation, J. Mater. Chem. 3 (2015) 4405–4412.
[79] W.-S. Hung, C.-H. Tsou, M. De Guzman, Q.-F. An, Y.-L. Liu, Y.-M. Zhang, C.-C. Hu, K.-R. Lee, J.-Y. Lai, Cross-linking with diamine monomers to prepare composite graphene oxide-framework membranes with varying d-spacing, Chem. Mater. 26 (2014) 2983–2990.
[80] Y. Qian, X. Zhang, C. Liu, C. Zhou, A. Huang, Tuning interlayer spacing of graphene oxide membranes with enhanced desalination performance, Desalination 460 (2019) 56–63.
[81] N. Meng, W. Zhao, E. Shamsaei, G. Wang, X. Zeng, X. Lin, T. Xu, H. Wang, X. Zhang, A low-pressure GO nanofiltration membrane crosslinked via ethylenediamine, J. Membr. Sci. 548 (2018) 363–371.
[82] W.-S. Hung, Y.-H. Chiao, A. Sengupta, Y.-W. Lin, S.R. Wickramasinghe, C.-C. Hu, H.-A. Tsai, K.-R. Lee, J.-Y. Lai, Tuning the interlayer spacing of forward osmosis membranes based on ultrathin graphene oxide to achieve desired performance, Carbon 142 (2019) 337–345.
[83] M. Zhang, Y. Mao, G. Liu, G. Liu, Y. Fan, W. Jin, Molecular bridges stabilize graphene oxide membranes in water, Angew. Chem. Int. Ed. 59 (2019) 1689–1695.
[84] K. Nakagawa, H. Yamashita, D. Saeki, T. Yoshioka, T. Shintani, E. Kamio, H. Kreissl, S. Tsang, S. Sugiyama, H. Matsuyama, Niobate nanosheet membranes with enhanced stability for nanofiltration, Chem. Commun. 53 (2017) 7929–7932.
[85] S. Kim, X. Lin, R. Ou, H. Liu, X. Zhang, G.P. Simon, C.D. Easton, H. Wang, Highly crosslinked, chlorine tolerant polymer network entwined graphene oxide membrane for water desalination, J. Mater. Chem. 5 (2017) 1533–1540.
[86] S. Kim, R. Ou, Y. Hu, X. Li, H. Zhang, G.P. Simon, H. Wang, Non-swelling graphene oxide-polymer nanocomposite membrane for reverse osmosis desalination, J. Membr. Sci. 562 (2018) 47–55.
[87] S. Park, K.-S. Lee, G. Bozoklu, W. Cai, S.T. Nguyen, R.S. Ruoff, Graphene oxide papers modified by divalent ions—enhancing mechanical properties via chemical cross-linking, ACS Nano 2 (2008) 572–578.
[88] A. Nicolaï, B.G. Sumpter, V. Meunier, Tunable water desalination across graphene oxide framework membranes, Phys. Chem. Chem. Phys. 16 (2014) 8646–8654.
[89] X. Qian, N. Li, Q. Wang, S. Ji, Chitosan/graphene oxide mixed matrix membrane with enhanced water permeability for high-salinity water desalination by pervaporation, Desalination 438 (2018) 83–96.
[90] Y. Wang, R. Ou, H. Wang, T. Xu, Graphene oxide modified graphitic carbon nitride as a modifier for thin film composite forward osmosis membrane, J. Membr. Sci. 475 (2015) 281–289.
[91] M. Safarpour, A. Khataee, V. Vatanpour, Thin film nanocomposite reverse osmosis membrane modified by reduced graphene oxide/TiO_2 with improved desalination performance, J. Membr. Sci. 489 (2015) 43–54.
[92] L. Jin, Z. Wang, S. Zheng, B. Mi, Polyamide-crosslinked graphene oxide membrane for forward osmosis, J. Membr. Sci. 545 (2018) 11–18.
[93] R. Hu, Y. He, C. Zhang, R. Zhang, J. Li, H. Zhu, Graphene oxide-embedded polyamide nanofiltration membranes for selective ion separation, J. Mater. Chem. 5 (2017) 25632–25640.
[94] X. Wu, M. Ding, H. Xu, W. Yang, K. Zhang, H. Tian, H. Wang, Z. Xie, Scalable $Ti_3C_2T_x$ MXene interlayered forward osmosis membranes for enhanced water purification and organic solvent recovery, ACS Nano 14 (2020) 9125–9135.
[95] N. Padmavathy, S.S. Behera, S. Pathan, L. Das Ghosh, S. Bose, Interlocked graphene oxide provides narrow channels for effective water desalination through forward osmosis, ACS Appl. Mater. Interfaces 11 (2019) 7566–7575.
[96] P. Sun, R. Ma, W. Ma, J. Wu, K. Wang, T. Sasaki, H. Zhu, Highly selective charge-guided ion transport through a hybrid membrane consisting of anionic graphene oxide and cationic hydroxide nanosheet superlattice units, NPG Asia Mater. 8 (2016) e259.
[97] W. Hirunpinyopas, E. Prestat, S.D. Worrall, S.J. Haigh, R.A. Dryfe, M.A. Bissett, Desalination and nanofiltration through functionalized laminar MoS_2 membranes, ACS Nano 11 (2017) 11082–11090.
[98] H. Li, T.-J. Ko, M. Lee, H.-S. Chung, S.S. Han, K.H. Oh, A. Sadmani, H. Kang, Y. Jung, Experimental realization of few layer two-dimensional MoS_2 membranes of near atomic thickness for high efficiency water desalination, Nano Lett. 19 (2019) 5194–5204.
[99] M. Deng, K. Kwac, M. Li, Y. Jung, H.G. Park, Stability, molecular sieving, and ion diffusion selectivity of a lamellar membrane from two-dimensional molybdenum disulfide, Nano Lett. 17 (2017) 2342–2348.
[100] L. Ries, E. Petit, T. Michel, C.C. Diogo, C. Gervais, C. Salameh, M. Bechelany, S. Balme, P. Miele, N. Onofrio, Enhanced sieving from exfoliated MoS_2 membranes via covalent functionalization, Nat. Mater. 18 (2019) 1112–1117.
[101] X. Xie, C. Chen, N. Zhang, Z.-R. Tang, J. Jiang, Y.-J. Xu, Microstructure and surface control of MXene films for water purification, Nature Sustain. 2 (2019) 856–862.
[102] B. Feng, K. Xu, A. Huang, Covalent synthesis of three-dimensional graphene oxide framework (GOF) membrane for seawater desalination, Desalination 394 (2016) 123–130.
[103] M. Zhang, J. Sun, Y. Mao, G. Liu, W. Jin, Effect of substrate on formation and nanofiltration performance of graphene oxide membranes, J. Membr. Sci. 574 (2019) 196–204.